Received: 11 October 2022 | Revised: 9 January 2023 | Accepted: 16 January 2023 | Published on: 6 February 2023

DOI: 10.1002/mrm.29609

REVIEW

Magnetic Resonance in Medicine

Update on state-of-the-art for arterial spin labeling (ASL) human perfusion imaging outside of the brain

Manuel Taso[1] | Veronica Aramendía-Vidaurreta[2] | Erin K. Englund[3] | Susan Francis[4] | Suzanne Franklin[5,6] | Ananth J. Madhuranthakam[7] | Petros Martirosian[8] | Krishna S. Nayak[9] | Qin Qin[10] | Xingfeng Shao[11] | David L. Thomas[12] | Zungho Zun[13] | Maria A. Fernández-Seara[2] | on behalf of the ISMRM Perfusion Study Group

Correspondence
Manuel Taso, PhD, Beth Israel Deaconess Medical Center Division of MRI Research – Dept. of Radiology 330, Brookline Avenue – Ansin 244, Boston, MA 02215, USA.
Email: mtaso@bidmc.harvard.edu

Funding information
NIH/NCATS, Grant/Award Numbers: AHA853697, KL2 TR002534, UL1 TR002535; NIH/NCI, Grant/Award Number: U01CA207091; NIH/NHLBI, Grant/Award Numbers: R01HL138182, R01HL144751; NIH/NICHD, Grant/Award Number: R01HD100012; Government of Navarra, Grant/Award Numbers: ERAPERMED2020-326-RESPECT, PC181-182-RM-RENAL; UCLH NIHR Biomedical Research Centre; Wellcome Trust, Grant/Award Number: 539208; Spanish Ministry of Science and Innovation, Grant/Award Number: PI21/00578

Abstract

This review article provides an overview of developments for arterial spin labeling (ASL) perfusion imaging in the body (i.e., outside of the brain). It is part of a series of review/recommendation papers from the International Society for Magnetic Resonance in Medicine (ISMRM) Perfusion Study Group. In this review, we focus on specific challenges and developments tailored for ASL in a variety of body locations. After presenting common challenges, organ-specific reviews of challenges and developments are presented, including kidneys, lungs, heart (myocardium), placenta, eye (retina), liver, pancreas, and muscle, which are regions that have seen the most developments outside of the brain. Summaries and recommendations of acquisition parameters (when appropriate) are provided for each organ. We then explore the possibilities for wider adoption of body ASL based on large standardization efforts, as well as the potential opportunities based on recent advances in high/low-field systems and machine-learning. This review seeks to provide an overview of the current state-of-the-art of ASL for applications in the body, highlighting ongoing challenges and solutions that aim to enable more widespread use of the technique in clinical practice.

KEYWORDS

arterial spin labeling (ASL), body MRI, perfusion imaging

1 | INTRODUCTION

Arterial spin labeling (ASL) perfusion imaging was originally developed for cerebral blood flow measurements.[1,2] From the beginning, it was clear that this technique bore tremendous advantages over contrast-based and/or ionizing methods, and would also be useful throughout the body.[3] In the 30 years since its introduction, ASL has become sufficiently mature to be used routinely for neurological applications, as highlighted by the 2015 "white

For affiliations refer to page 1770

paper" which set recommendations and guidelines for clinical use.[4]

Body ASL, herein defined as application of ASL to any part of the human body outside of the brain, is a work-in-progress and not yet suitable for routine clinical use. This is in part due to unique application-specific imaging challenges. But the desire for exogenous contrast-free perfusion imaging outside of the brain is very high because of the promise of a method capable of providing absolute, reproducible, and quantitative blood flow measurements, which would be potentially useful in a variety of applications including oncology, nephrology, cardiology, endocrinology, and many others. Particularly, ASL is a promising MRI alternative in cases where dadolinium (Gd)-based contrast agents cannot be administered due to contra-indications as well as in the context of recent concerns regarding Gd retention, which further justifies seeking non-contrast alternatives.[5]

This paper seeks to offer a comprehensive review of recent advances in human perfusion imaging with ASL outside of the brain. After reviewing some of the common challenges associated with using ASL in the body, organ-specific challenges and developments are presented covering the majority of extracranial ASL applications. In addition, national and international initiatives are highlighted which promote the use of ASL for body applications by offering technical recommendations and standardization guidelines, ending with a discussion on potential future directions for body ASL in the years ahead. This manuscript is part of a wider effort arising from the International Society for Magnetic Resonance in Medicine (ISMRM) Perfusion Study Group meeting in 2020. Indeed, several years after the original ASL "white paper" for brain imaging, the ASL imaging community identified the need to provide an updated perspective on various aspects of ASL technical development and use.

2 | GENERALITIES AND COMMON CHALLENGES IN BODY ASL

2.1 | ASL methods summary

ASL uses arterial blood water as an endogenous tracer, by modifying the longitudinal magnetization of arterial blood with RF pulses and gradient fields. Throughout this review, three labeling methods are addressed as highlighted in Figure 1:

- Pulsed ASL (PASL), using short (≈10 ms) single time-point inversion pulses applied to a large volume of blood with varying control strategies.
- (Pseudo)-continuous ASL (CASL/PCASL), using flow-driven adiabatic inversion through a labeling plane during longer periods of time (≈1–2 s) compared to PASL.
- Velocity-selective ASL (VS-ASL), exploiting velocity selectivity rather than spatial selectivity to achieve labeling.

2.2 | Challenges in body ASL

The implementation of ASL in the chest and abdomen is often hindered by physiological motion, such as myocardial motion between systolic and diastolic cardiac phases, respiration-induced movement during exhalation and inhalation, and peristalsis of the gastrointestinal tract with involuntary constriction and relaxation. Acquiring data from moving organs inevitably leads to displacement and blurring of images. Recorded abdominal organ motion throughout respiration showed averaged displacements of kidney, liver, and spleen of 1.10–1.30 cm, 0.14–0.25 cm, and 0.44–0.61 cm in superior–inferior, left–right, and anterior–posterior directions, respectively.[6] Varying motion effects between label and control ASL images result in mismatch of the paired raw images and subsequent subtraction errors in qualitative and quantitative perfusion maps.

Furthermore, the descending aorta typically exhibits large variations of flow velocities through cardiac cycles, ranging from 40 to 120 cm/s during systole to <10 cm/s during diastole,[7,8] with occurrences of retrograde flow.[9] This is likely to considerably reduce ASL labeling efficiency, especially with flow-driven adiabatic inversion methods (e.g., PCASL).[10]

The sensitivity to off-resonance (B_0) and RF transmit (B_1^+) inhomogeneities limit the performance of body ASL at high field. The main source of B_0 inhomogeneities in the body are air spaces for example the alveoli in the lungs or air in the intestines. Large B_0 offsets are primarily displayed within the chest and near the lung–liver interface, which can lead to image dropout and distortion, as well as reducing the labeling efficiency. The macroscopic frequency shift of the lung can be up to 3.6 ppm relative to adjacent myocardial or esophageal muscle.[11] The maximal respiration-induced B_0 field fluctuation has been shown to reach 0.6 ppm at the lower cervical spinal cord.[12]

The B_1^+ field inhomogeneities within the abdomen are influenced by both body geometry and tissue composition. Due to the RF wavelength shortening in water-containing tissue, more severe B_1^+ inhomogeneity could be induced at higher field strength by larger body size with less fat fraction.[13,14] B_1^+ drops up to −40% to 70% of prescribed flip-angles at 3T have been measured in some areas of the heart,[15] kidney,[16] and breast[17] as illustrated in Figure 2. This again will cause inaccuracies in blood

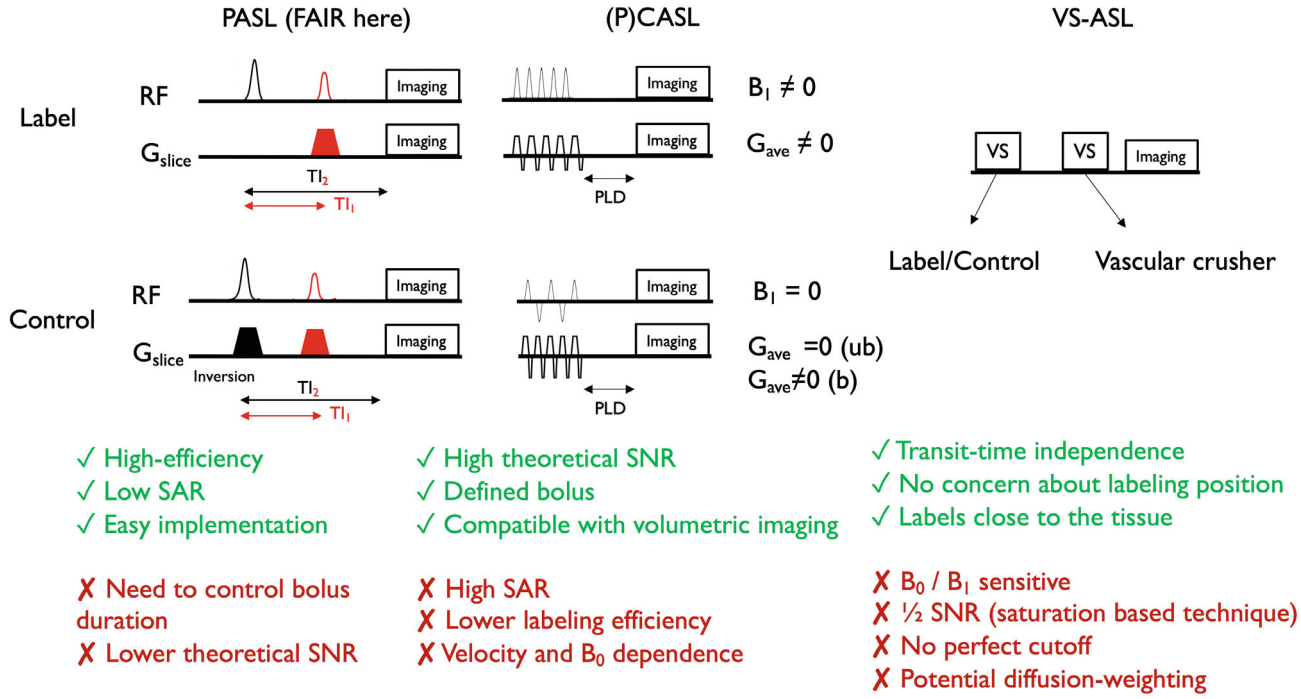

FIGURE 1 Illustration of FAIR, PCASL, and VS-ASL as well as advantages/drawbacks of the different labeling methods

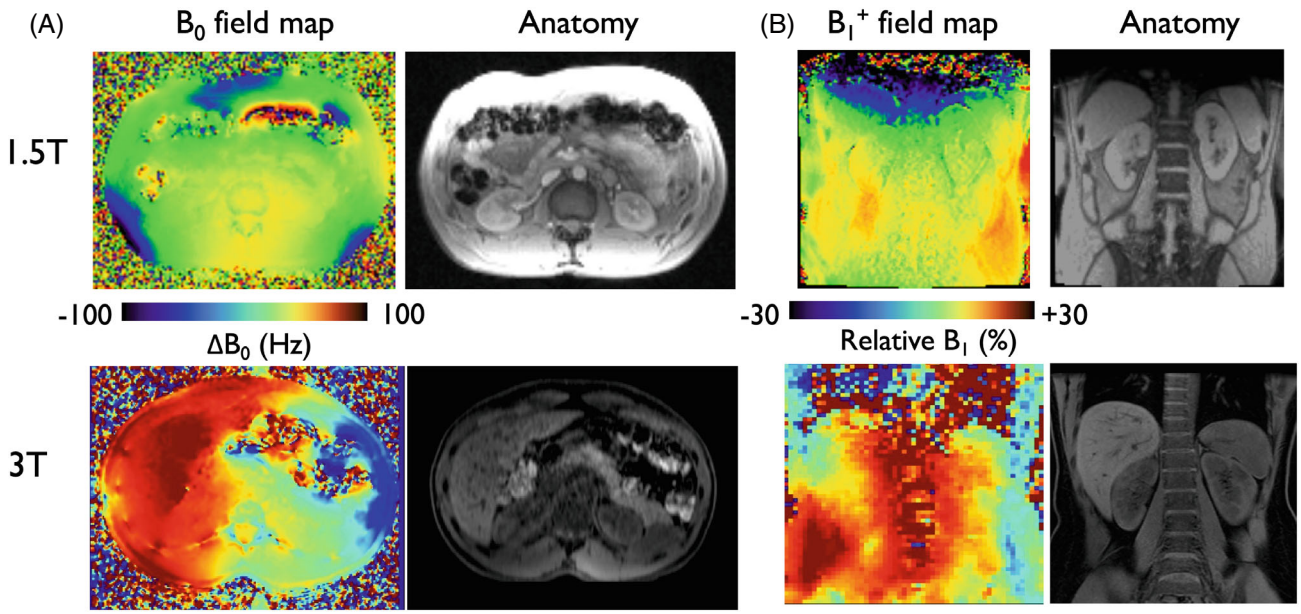

FIGURE 2 Illustration of B_0/B_1 distributions in the abdomen in two different volunteers at 1.5T (top) and 3T (bottom)

flow quantification, and therefore must be addressed appropriately.

3 | ASL IN SPECIFIC ORGANS

This section offers a review of ASL challenges and developments in specific organs and anatomical regions.

3.1 | Kidneys

The kidneys are abdominal organs supplied by the renal arteries that branch directly from the abdominal aorta, below the celiac trunk. They are unique organs, in that perfusion drives metabolic activity rather than the opposite. With reduced perfusion, the glomerular filtration rate (GFR) decreases,[18] reducing the kidneys' vital task of

filtering excess fluid and waste products from the blood. Currently, abnormal GFR is the most accepted measure to define and diagnose kidney pathology,[19,20] but its usefulness is limited because it is a global measure of kidney function. Perfusion imaging enables evaluation of local kidney function. However, the use of contrast agents is restricted in patients with severe chronic kidney disease (CKD), acute kidney injury (AKI), or in patients who have previously experienced a severe reaction to contrast material,[21] making ASL particularly valuable in kidney applications.

Another important characteristic of the kidney is the presence of two compartments: cortex and medulla, with circulations that are independently regulated.

3.1.1 | Challenges

There are three major factors that affect ASL measurements in the kidneys: B_0 and B_1 inhomogeneities and motion. The first two can degrade the labeling efficiency, especially for PCASL, because of the necessary proximity of the labeling plane to the lungs. PCASL efficiency is also affected by the fast and highly pulsatile flow in the abdominal aorta.[22] When considering FAIR labeling, the proximity of the aorta to the kidneys must be carefully checked for positioning.

Respiratory motion is a challenge common to all abdominal organs. The kidneys move in a tilted orientation, with the largest motion being in the craniocaudal direction and varying from a few mm to 2–3 cm during normal respiration.[23] This can generate subtraction errors due to the organ displacement between label and control images in single-shot 2D acquisitions and also hamper the use of long or segmented 3D readouts.

Another challenge specific to the kidney is to obtain reliable measurements in the medulla because of lower flow and longer transit time relative to the cortex, which both result in reduced SNR and partial volume contamination with the cortical signal.

3.1.2 | Developments

The kidney is the extracranial body organ where ASL has been most successful due to the high perfusion levels in the renal cortex. Several comprehensive reviews of renal ASL studies have been published[18,24,25]; therefore, we will limit our reporting to the current developments. A recent consensus paper by an expert panel reported guidelines for clinical translation of renal ASL,[26] with the goal of promoting the widespread standardized use. To that end, the panel proposed a default protocol, considered robust and reproducible for most applications presented in the Recommendation section below.

Optimization of PCASL parameters specifically for renal applications has been shown to considerable improve labeling efficiency.[22] The "unbalanced" implementation of PCASL is more robust to field inhomogeneity at the labeling location, compared to the "balanced" approach[27] although eddy current differences between label/control are minimized in balanced PCASL. Studies directly comparing PCASL and FAIR have yielded mixed results.[28,29] An exhaustive comparison between FAIR and a kidney optimized PCASL implementation is warranted.

An alternative labeling approach is VS-ASL, which has shown promising results[30] despite lower temporal SNR (tSNR) than spatially selective approaches.[31] Velocity-selective inversion prepared ASL (VSI-ASL), where labeling of blood is based on inversion of the magnetization, is the most promising technique in terms of SNR in brain,[16,32] although issues with B_0 robustness need to be addressed for renal applications.[16] Recent developments to improve robustness to field inhomogeneities include dynamic phase cycling[33] and use of a motion-insensitive control module (instead of motion-compensated).[32,34] However dynamic phase cycling is likely not suitable for moving organs like the kidneys, because it depends on spatial averaging of signal over dynamics.[33]

Various 3D readout approaches have been proposed to address the challenges of long acquisition times, movement between segments, and off-resonance sensitivity.[35–37] Different approaches have been reported to reduce the acquisition time of 3D-FSE readouts, while maintaining robustness to off-resonance. Taso et al. combined 3D-FSE with Compressed-Sensing[37] while Greer et al. implemented 3D-FSE with Cartesian acquisition and spiral profile reordering (CASPR).[36] In addition, single-shot 3D-GRASE was optimized for pediatric patients, with shorter scan time and thus less motion sensitivity, achieved at the cost of imaging resolution.[35] Figure 3 shows two example datasets acquired using PCASL with both SE-EPI and SSFSE readouts.

With regard to quantification, although single timepoint methods can accurately measure cortical blood flow, provided that the entire labeled bolus is delivered to the tissue,[4] multiple timepoint strategies (e.g., multi TI/PLD) methods have also been implemented mostly relying on FAIR labeling,[38,39] yielding simultaneous blood flow and transit-time measurements that can be valuable in patient populations with slowed and/or delayed flow. An extensive detailed list of ASL studies and blood flow ranges can be found in an earlier review[18] with a range of cortical blood flow measures found between 139 and 427 ml/100 g/min.

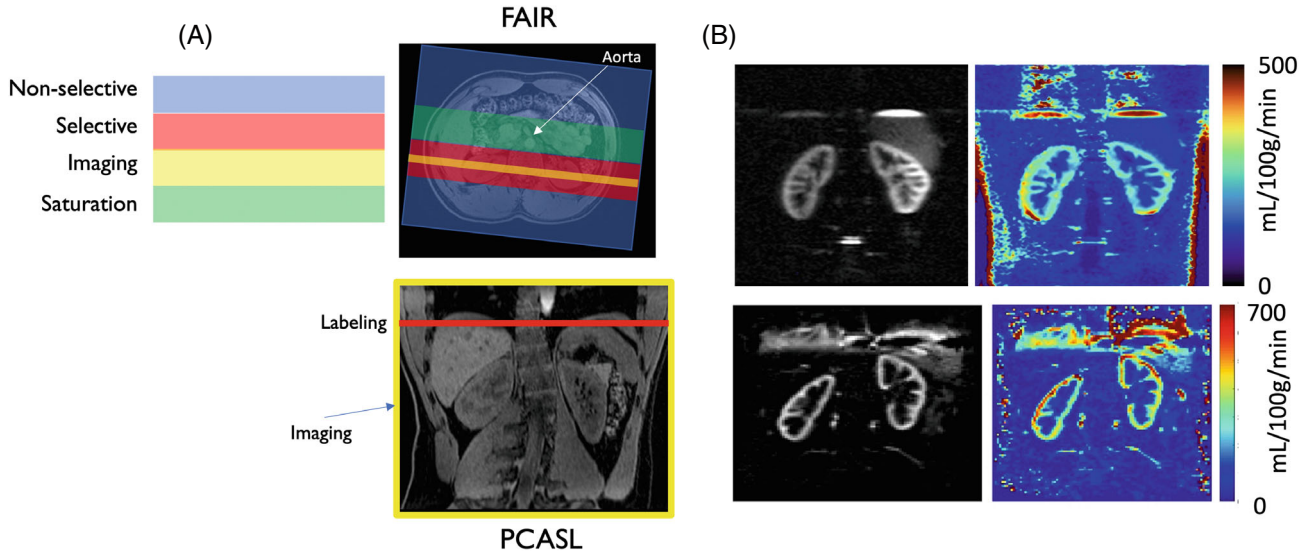

FIGURE 3 (A) Illustration of labeling geometry for FAIR and PCASL experiments. (B) Two sets of ASL difference and quantitative RBF acquired with a PCASL-SSFSE sequence at 3T (top) and PCASL SE-EPI at 3T (bottom) in two different healthy volunteers on two different scanners

3.1.3 | Recommendations

Following the PARENCHIMA initiative detailed later in this manuscript, the following are recommended:

- Both FAIR and PCASL are adequate labeling methods for renal imaging.
- if PCASL is used, the 'unbalanced' implementation is recommended for robustness to B_0 offsets, with labeling positioned 8–10 cm above the kidneys in the descending aorta.
- Spin-echo EPI is the recommended readout as it is widely available across platforms, although other readouts such as SSFSE or bSSFP have also been successfully used and shown satisfactory results.
- Coronal oblique acquisitions are recommended.
- Free-breathing acquisitions with retrospective realignment for motion-correction.
- Single timepoint (i.e., TI or PLD) imaging with single compartment modeling is recommended for its ease of use.
- Only cortical blood flow should be reported as medullary blood flow measurements are not considered reliable.

3.2 | Lungs

Lungs perform an essential function in delivering oxygen and removing carbon-dioxide from the blood, through the perfusion of the lungs. In contrast to other organs, perfusion of the lungs is achieved by deoxygenated blood from the right ventricle of the heart. Variations in perfusion and/or ventilation cause compromised lung function in diseases such as chronic obstructive pulmonary disorders (COPD) and pulmonary embolism (PE). Planar scintigraphy or contrast-enhanced computed tomography (CT) are often used to measure lung perfusion, but these approaches suffer from exposure to ionizing radiation. This is of significant concern for longitudinal monitoring, particularly in younger and pediatric patients. Non-contrast perfusion measurement using ASL provides an ideal strategy enabling perfusion imaging across a broader age group and repeated measurements for quantitative assessments without requiring contrast administration, as highlighted in pioneering studies which demonstrated the utility of ASL perfusion in the lungs to understand lung physiology[40] and characterize various pathologies such as cystic fibrosis.[41]

3.2.1 | Challenges

Pulmonary ASL is particularly challenging due to several factors. The highly pulsatile blood flow combined with the complex anatomy of the pulmonary vasculature makes it challenging to achieve high labeling efficiency and collect data with minimal contribution of intravascular signal. In addition, the low proton density of the lungs reduces the SNR. The presence of air/tissue interfaces also degrades image quality because of susceptibility-induced

dropouts especially with gradient-echo and EPI acquisitions. Finally, both cardiac and respiratory motion have to be considered when designing acquisitions.

3.2.2 | Developments

Because of these challenges, the majority of the ASL work in lungs has been performed at 1.5T and below[41] using mostly SSFSE acquisitions[37] and global labeling strategies (e.g., FAIR).[39,40] Because of the potential impact of cardiac cycle on imaging signal, cardiac gating has been used especially for SSFSE.[42]

Because of the complex vascular anatomy, a strategy relying on PCASL labeling in the inferior vena cava (IVC) to measure lung perfusion was also proposed. However, the long transit time from IVC to the lungs combined with variations in the heart rate contributed to random signal variations beyond perfusion. Nevertheless, this approach has shown clinical value in single ventricle patients who had undergone Fontan procedure to measure the differential perfusion to the lungs.[43] Subsequent developments included labeling the right pulmonary artery (RPA) combined with background suppression to improve the SNR and image robustness. This labeling strategy has been used in combination with cardiac-triggered bSSFP acquisitions at 1.5T[44] and SSFSE at 3T.[45] Challenges associated with reduced PCASL labeling efficiency due to B_0 inhomogeneities are more relevant for this RPA labeling and could benefit from unbalanced PCASL labeling approaches, which increases off-resonance robustness. Recently, a combination of ECG-triggered PCASL of the main pulmonary artery and bSSFP readout at 1.5T enabled perfusion imaging of the lung even under free-breathing.[44]

Low SNR has necessitated multiple signal averages and prolonged acquisition times, thus the majority of prior ASL lung perfusion studies were restricted to a single slice. Recent advances using optimized background suppression has enabled multi-slice acquisitions during free-breathing using FAIR to cover the entire lungs in <5 min of acquisition time.[46] This approach has demonstrated clinical utility in measuring lung perfusion in pediatric patients with PE[47] and could be potentially used in longitudinal monitoring without the concerns of Gd contrast administration or exposure to ionizing radiation.

Figure 4 shows a dataset acquired with a FAIR-SSFSE sequence at 3T in a healthy volunteer.

3.2.3 | Summary

Lung ASL perfusion imaging is still a heavily research-oriented technique, therefore recommendations are premature. However, the following can be summarized:

- Both FAIR and PCASL have been implemented and shown to be feasible, although careful planning of labeling plane positioning has to be considered for PCASL as highlighted in Figure 4.
- Because of susceptibility effects, 1.5T field strength has been more widely used in lung ASL studies.
- Non-EPI readouts such as SSFSE and bSSFP are heavily favored.

3.3 | Placenta

The placenta plays an important role in delivery of oxygen and nutrients from the mother to the fetus during pregnancy. Early in pregnancy, migration of trophoblast cells to the lumen of the spiral arteries in the uterus leads to 5- to 10-fold terminal dilation of the arteries, thereby supplying adequate blood flow required for normal fetal development.[48] Abnormal placentation associated with

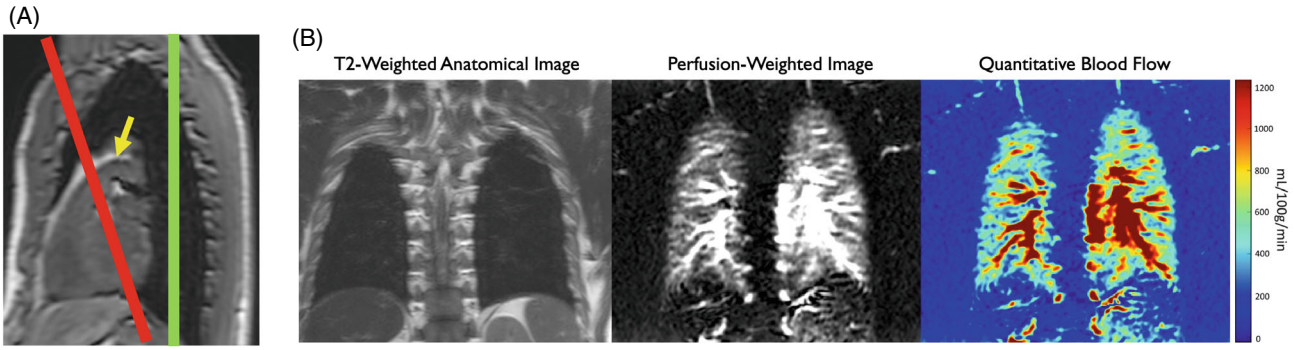

FIGURE 4 (A) Schematic showing the positioning of the labeling plane for pCASL (red) over the main pulmonary artery (arrow) and the coronal imaging slice (light green) for lung perfusion imaging. For FAIR, the selective labeling is also applied across the imaging slice (light green). (B) Example of dataset acquired with a FAIR-SSFSE sequence at 3T in a healthy volunteer

failure of this conversion of spiral arteries results in the condition of placental insufficiency, which is the most common cause of maternal-fetal complications such as fetal growth restriction and preeclampsia. Measurement of placental perfusion therefore may be used for early detection of placental insufficiency. ASL is well suited for such measurements because it does not require contrast agents, which are contraindicated during pregnancy.

3.3.1 | Challenges

The main challenge of placental ASL with spatially-selective labeling is to determine the optimal labeling region. The major path of maternal arterial blood flow to the placenta is via the descending aorta, internal iliac arteries, and uterine arteries. There is also another route from the descending aorta to the ovarian arteries, which accounts for about 15% of maternal-placental circulation.[49] Both of these arterial paths are highly circuitous and complex. Coupled with variation in location and shape of the placenta across subjects, labeling in the descending aorta may be necessary to capture all these inflow contributions without detailed, subject-specific labeling positioning, However, this location may be a significant distance from the placenta, leading to SNR loss due to signal decay during the potentially long transit-time. Slower blood velocity (~11.5 cm/s) in the descending aorta may also affect the labeling efficiency of PCASL (~77%),[50] unless the PCASL labeling pulses are modified to account for this.

3.3.2 | Developments

The first placental ASL study was reported more than two decades ago using FAIR labeling and Look-Locker imaging on a single slice.[51] More recently, the Human Placenta Project (HPP) launched by the National Institute of Child Health and Human Development[52] has prompted multiple placental ASL studies from different research groups, which utilized more advanced forms of labeling and imaging methods.[50,53–59] Application of PCASL in the placenta was a logical choice and was demonstrated using a labeling plane placed at the bifurcation of the descending aorta to selectively label maternal placental perfusion.[50] In a follow-up study using this approach, high-risk pregnancies manifested significantly lower placental perfusion than healthy pregnancies in regions with high placental perfusion, which are mainly the center of the placental lobules.[59]

Another labeling approach for the placenta that was studied in parallel with PCASL was VS-ASL, in which signal is sensitive to the movement of blood even within the placenta and is contributed to by both maternal and fetal flow.[54,55,57,58] The initial study on the feasibility of placental VS-ASL demonstrated that ASL SNR was significantly higher in VS-ASL than PCASL.[55] A clinical study of placental VS-ASL also showed that global placental perfusion significantly decreased with advancing gestational age in pregnancies complicated with fetal heart disease whereas there was no association between placental perfusion and gestational age in healthy pregnancies.[54] Placental VS-ASL was further studied to optimize acquisition parameters, such as cut-off velocity, velocity encoding direction, and inflow time.[58] In addition, VS-ASL has been combined with T2* mapping, enabling simultaneous measurement of perfusion and oxygenation.[57]

Figure 5 shows examples of placental images acquired with PCASL and VS-ASL in normal pregnancies.

3.3.3 | Summary

The feasibility of both PCASL and VS-ASL in the placenta have been successfully demonstrated and their potential for detecting abnormal placental perfusion in small cohorts has been reported. Follow-up studies are warranted in a large-scale clinical setting to determine whether these approaches can be used as early screening and diagnostic tools for identifying pregnancies at risk. A list of placental perfusion studies is summarized in Table S1.

3.4 | Heart (i.e., Myocardium)

Myocardial perfusion is an important index for the assessment of coronary artery disease, one of the most common causes of cardiovascular related deaths.[60,61] As a first sign of the ischemic cascade, perfusion abnormalities can be detected earlier during hyperemia, when healthy coronary arteries experience an increase of three to five times the resting blood flow but diseased vessels do not.[62] This leads to a reduction in the ratio of stress to rest perfusion, known as myocardial perfusion reserve (MPR), which is a critical parameter for the detection of significant coronary stenosis. Patients with suspected coronary artery disease are often referred for a first-pass stress-rest cardiac MRI study in which the injection of at least two doses of Gd contrast agent is required.

3.4.1 | Challenges

The main obstacles to the application of ASL in the heart include the difficulty in labeling blood prior to entering

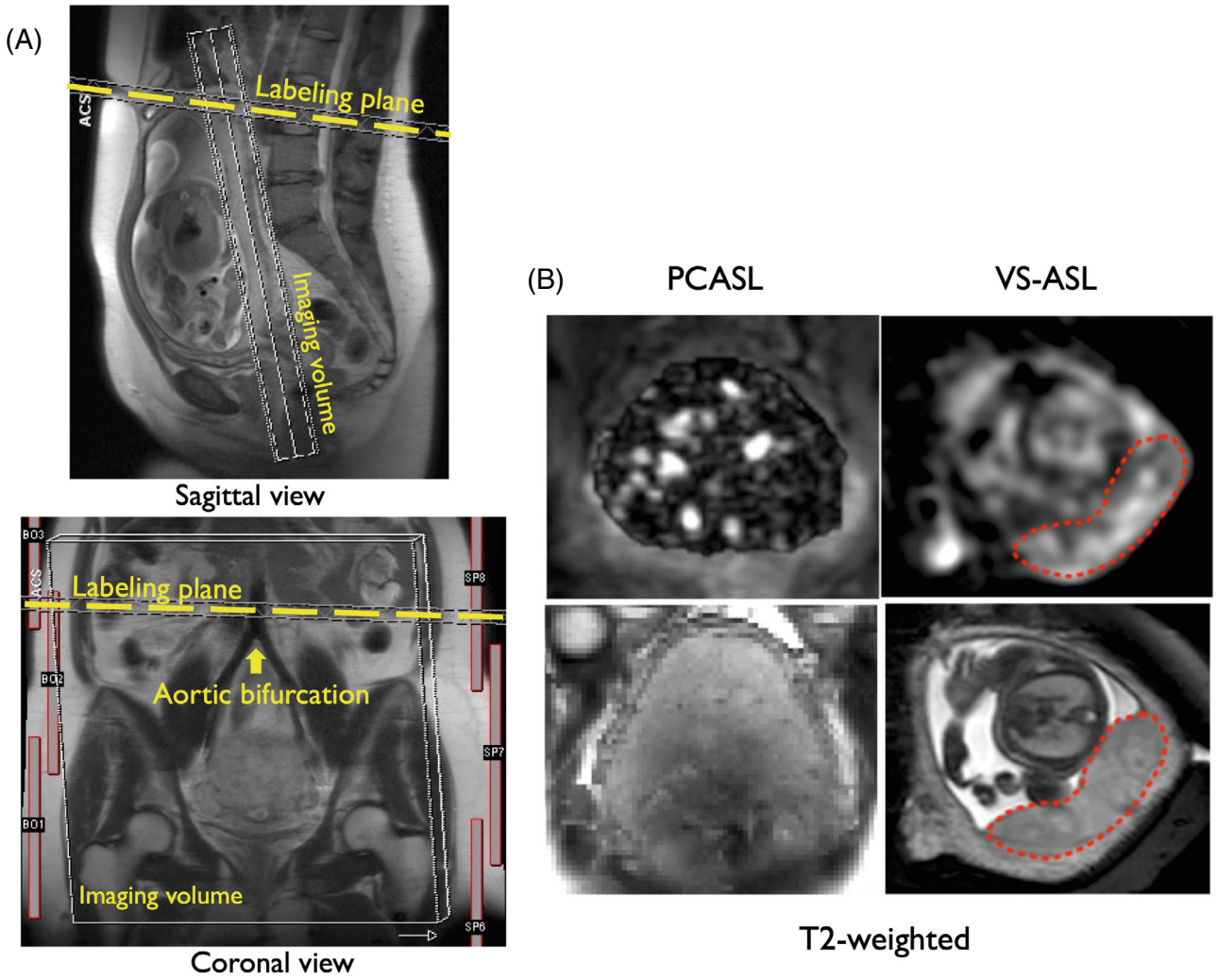

FIGURE 5 (A) Placenta PCASL planning. (B) ASL images acquired using PCASL and VS-ASL (top) and corresponding T2-weighted anatomical images (bottom) modified from Shao et al. 2018 and Zun et al. 2017 (reproduced under a Creative Commons Attribution 4.0 International License - http://creativecommons.org/licenses/by/4.0/)

the coronary arteries due to the circuitous path of blood through the heart, the presence of both cardiac and respiratory motion, and the short scan time available during peak vasodilation.[63]

3.4.2 | Developments

Most studies have used FAIR as labeling method. Quantification models fall into two groups, known as intensity difference[64] and apparent T_1[65] approaches. The first employs the intensity difference between label and control images acquired at a single TI for quantification, assuming that the T1 of blood and myocardium are nearly equal. In this context, both single[66–70] and double[71–74] ECG gating techniques have been used. The former allows gating of the readout to a particular cardiac phase with the use of a fixed TI. Double ECG gating allows gating of both labeling and readout to the same cardiac phase separately, which is more robust to heart rate variations but leads to T variability that must be considered for quantification. The apparent T_1 approach requires the acquisition of images at different TIs, selected as an integer number of the RR interval.[75–78] Quantification is based on the myocardial T_1 ratio between control and label conditions. This approach allows the simultaneous quantification of arterial transit time, which has been estimated to be ~400 ms in healthy subjects.[77] Different respiratory strategies have been used to minimize motion, such as breath-holding,[66–68,78,79] synchronized-breathing,[70,71] navigator-gating or free-breathing combined with motion correction,[69,77,80] and segmentation[81] algorithms.

Myocardial FAIR ASL has been validated in a porcine model by comparison to radiolabeled microspheres,[71] showing the strongest correlation in the septum ($r = 0.86$) and the weakest in the anterior wall ($r = 0.67$). In human

studies, perfusion measurements obtained at rest are in agreement with the ranges published in PET.[82]

Various technical improvements have been published in healthy subjects. Scan time efficiency of free-breathing FAIR ASL was improved using a TR of ~4 s, which had similar mean signal and tSNR compared to longer TR sequences, allowing the acquisition of more images in the same scan time.[69] Systolic and diastolic perfusion measurements have been compared using compressed-sensing techniques in combination with a bSSFP readout.[74] EPI readout has been shown to facilitate the coverage of three myocardial slices (basal, midventricular, and apex), at the expense of lower tSNR than that obtained with bSSFP.[73]

The validity of myocardial FAIR ASL to detect hyperemia in healthy subjects has been tested with mild forms of stress[66,77,83] and pharmacological vasodilation.[68,76,84] In the clinical setting, ASL has been shown to detect an MPR reduction in patients with suspected coronary artery disease in agreement with invasive coronary angiography between anterior and posterior myocardium,[76] between normal and the most ischemic segments,[67] and between normal and hypoperfused segments (including both ischemic and infarcted), in correlation with semi-quantitative first-pass imaging.[70]

In addition to FAIR, other labeling strategies have been investigated. Steady-pulsed ASL[85] was implemented by labeling a thin slab covering the aortic root, followed by a bSSFP readout within the same cardiac cycle. Control scans were acquired with the labeling slab positioned symmetrically to the imaging slice. This allowed a more specific labeling of arterial blood perfusing the myocardium at every cardiac cycle improving scan efficiency. VS-ASL[34,86] was applied to avoid signal loss in the presence of slow flow and long transit delays. Labeling pulses were optimized for this particular application to achieve higher efficiency and prevent labeling of the moving myocardium. Myocardial ASL studies to date are summarized in Table S2. An example dataset using a FAIR-bSSFP sequence is shown in Figure 6.

3.4.3 | Summary

- FAIR, steady-pulsed, and VS approaches have been successfully applied to quantify myocardial perfusion. In

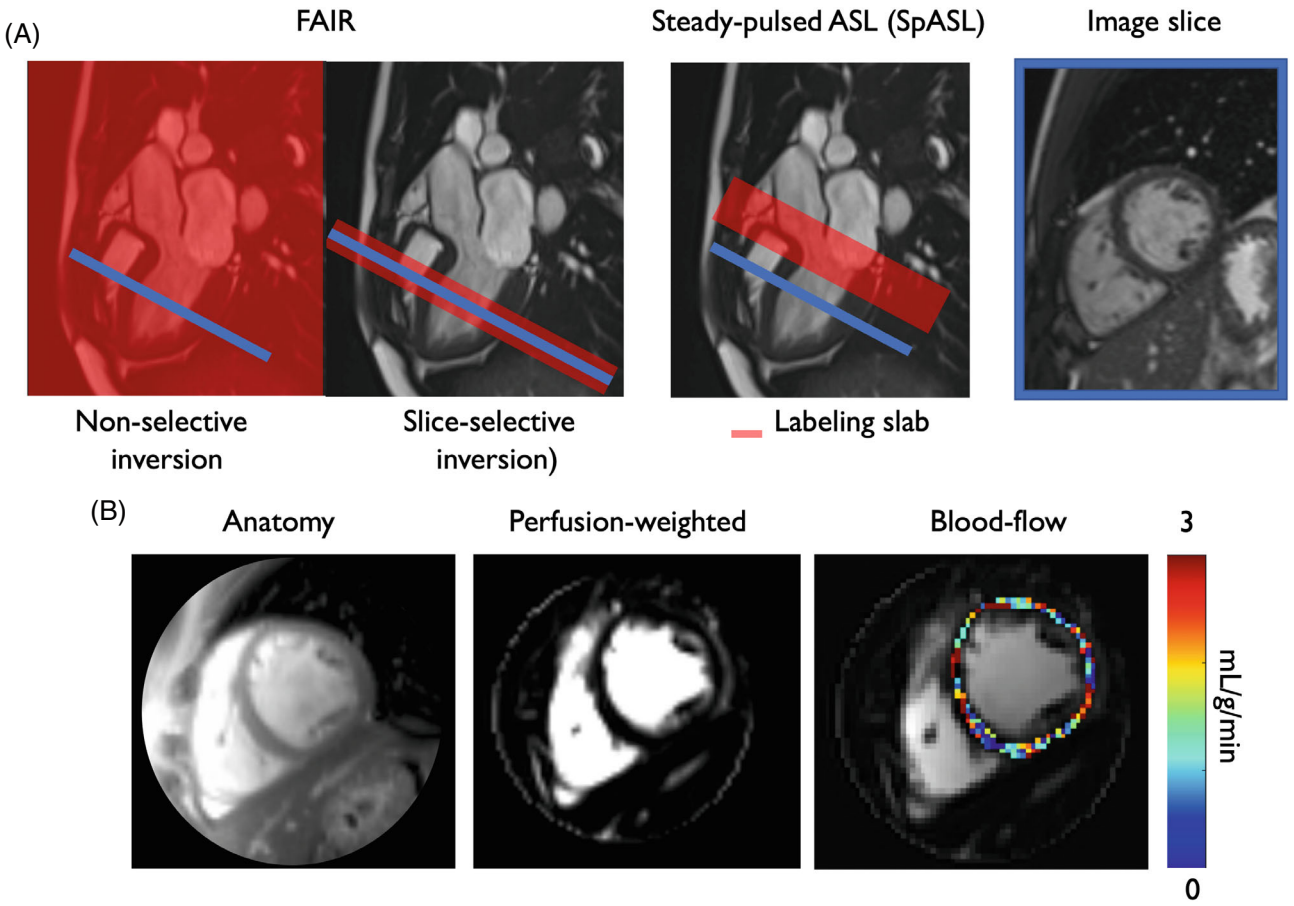

FIGURE 6 (A) Labeling geometry for myocardial FAIR and steady-pulsed ASL. (B) Illustration of anatomy, perfusion-weighted, and quantitative myocardial blood-flow in a healthy volunteer using a FAIR-bSSFP sequence at 3T

addition, FAIR has revealed its potential to detect hyperemic changes in the clinical practice.

- Further research on the development of myocardial ASL should be undertaken to allow for whole-heart coverage, automated analysis and improved sensitivity; these technical advances need to be achieved before it can replace first-pass perfusion measurements in the clinical setting.

3.5 | Liver

The liver is one of the largest internal organs in the human body, composed of two lobes of unequal size and shape. It is a vital organ, involved in multiple metabolic functions. Liver diseases (both diffuse and focal) are relatively frequent and imaging perfusion is crucial for their detection and characterization. MRI, in particular contrast-enhanced techniques, play an important role in the clinical evaluation of liver disease.

3.5.1 | Challenges

Liver perfusion imaging raises the unique challenge of a dual blood supply coming from the hepatic artery and the portal vein, which present anatomical variants across individuals.[87,88] The common hepatic artery branches from the aorta and delivers oxygenated blood to the liver parenchyma, which constitutes about 25% of the total liver supply, while the other 75% comes from the portal vein, a low pressure, high capacity vessel, which delivers deoxygenated blood and nutrients with slower blood flow.[89]

There is clinical interest in obtaining separate measurements of hepatic and portal perfusion because liver disease can affect both the global and relative flow rates in the two vessels.[90] When labeling blood in the portal vein, the blood is not arterial but venous; however ASL acronyms are still used in the text below.

3.5.2 | Developments

Hepatic ASL reports are sparse. The first attempt used CASL at 1.5T[91] to separately label arterial and venous blood. Arterial blood was labeled at the aorta by placing the labeling plane in suprahepatic axial orientation. Venous blood was labeled using a left medial sagittal plane that mainly labeled the splenic vein blood flow. A third labeling plane in right medial sagittal orientation was used to simultaneously label blood in the portal vein and hepatic artery to obtain a global perfusion measurement. Results of this preliminary study were promising, although venous flow measurements were underestimated.

Hoad et al. reported measurements of total liver perfusion and transit times using FAIR.[92] Although intra-subject reproducibility in healthy subjects was good, there was a wide inter-subject variation in blood flow, in both healthy and chronic liver disease populations. This technique was subsequently used to evaluate patients with compensated and decompensated cirrhosis, demonstrating a significant decrease in perfusion compared to healthy controls.[93] A similar approach combined with a multiphase Look-Locker sampling scheme was employed to assess hepatic hemodynamic changes and their correlation with portal hypertension[94] and to study alterations in liver perfusion due to physiological stress challenges.[95]

Portal perfusion measurements were reported by Katada et al., using multi-delay PASL-PICORE with Q2TIPS to selectively label the mesenteric and portal venous area, avoiding the celiac trunk.[96] Portal perfusion signal reached a peak value at TI = 3 s. The MR measurements were compared with CT perfusion during superior mesenteric artery portography, yielding a significant fair correlation, even though MR values were systematically higher than CT values.

Using two different sequences, PASL-EPISTAR and PCASL, Schalkx et al. were able to quantify portal venous and arterial perfusion in separate acquisitions.[97] EPISTAR was employed to label the venous blood (with an oblique labeling slab positioned caudal of the liver covering the portal vein and its feeding vessels and a TI = 2500 ms), while PCASL was used to label the arterial blood in the descending aorta (with a PLD = 1500 ms), to avoid re-tagging of spins after incomplete relaxation in the lungs and the heart. Using this strategy, the authors showed a significant increase in portal perfusion after meal intake, and a good correlation between portal perfusion measured with ASL and phase contrast. However, the challenge of measuring hepatic arterial flow was revealed by the low relative signal changes (ΔM) of $0.12 \pm 0.08\%$ and $0.08 \pm 0.11\%$ pre and post meal intake respectively.

Two separate multi-delay PCASL acquisitions were employed by Pan et al.[98] to quantify portal venous and arterial perfusion at 3 T. During the first acquisition, the labeling plane was located approximately perpendicular to the suprahepatic descending aorta, to label the blood in the hepatic artery, while for the second, the labeling plane was positioned approximately perpendicular to the portal vein, but also intersected the hepatic artery and descending aorta. In this configuration, arterial blood experienced a double inversion, resulting in minimal labeling.

Two PCASL acquisitions were also used by Martirosian et al.[99] In this case, first the labeling plane was positioned intersecting the portal vein and hepatic artery (nearly parallel to the aorta) to measure total flow, while for the second scan the labeling plane was below the hepatic

artery, intersecting the superior and inferior mesenteric and splenic veins to measure portal venous flow. Arterial perfusion was then computed by subtraction. In this work, background suppression was implemented, and transit time measurements were performed with multiple PLDs. Liver ASL studies to date are summarized in Table S3 and an example dataset is shown in Figure 7 using a PCASL-EPI sequence.

3.5.3 | Summary

- PASL and PCASL approaches can be used to measure total liver perfusion. However, PCASL is the method of choice for the separate estimation of portal and / or arterial perfusion.
- Because of the short liver T_1, multiple timepoints and more complex models can be used for accurate perfusion quantification.
- Background suppression and retrospective motion correction are strongly recommended, especially in free-breathing examinations.

3.6 | Eye (i.e., retina)

The retina, an extremely thin organ, receives its blood supply through two branches of the ophthalmic artery: the central retinal artery that is its primary source of blood and irrigates the inner retinal layers (known as retinal circulation), and the posterior ciliary arteries, which feed the outer layers of the retina (choroidal circulation).

3.6.1 | Challenges

Imaging retinal perfusion is challenging due to the organ thinness that requires high spatial resolution, the large magnetic field gradients in the eye area caused by air in the nearby sinuses and the motion of the eye globe. Retinal blood flow imaging has high clinical potential as most retinal pathologies are associated with perfusion irregularities.

3.6.2 | Developments

Alsop et al. first evaluated the feasibility of imaging human retinal perfusion[100] in a preliminary study at 1.5T using multi-delay FAIR with a 2D SSFSE readout, to reduce susceptibility effects, and heavy background suppression, to minimize motion artifacts.

Employing a similar readout strategy, with strong background suppression, retinal flow measurements were demonstrated at 3T using multi-delay PCASL as highlighted in Figure 8.[101] An axial labeling plane was positioned 5 cm beneath the level of the optic nerve, to label blood in the carotid and other arteries below the Circle of Willis. Images were acquired in a single axial slice passing through the optic nerve heads. Perfusion signal peaked for PLD = 1500 ms. Absolute blood flow was calculated per unit area by fitting the ASL signal as a function of time delay. With this technique vascular reactivity in the retina has also been assessed, using induced hypercapnia.[102]

A custom-made receiver eye coil was used to improve SNR and achieve high in-plane spatial resolution by Peng

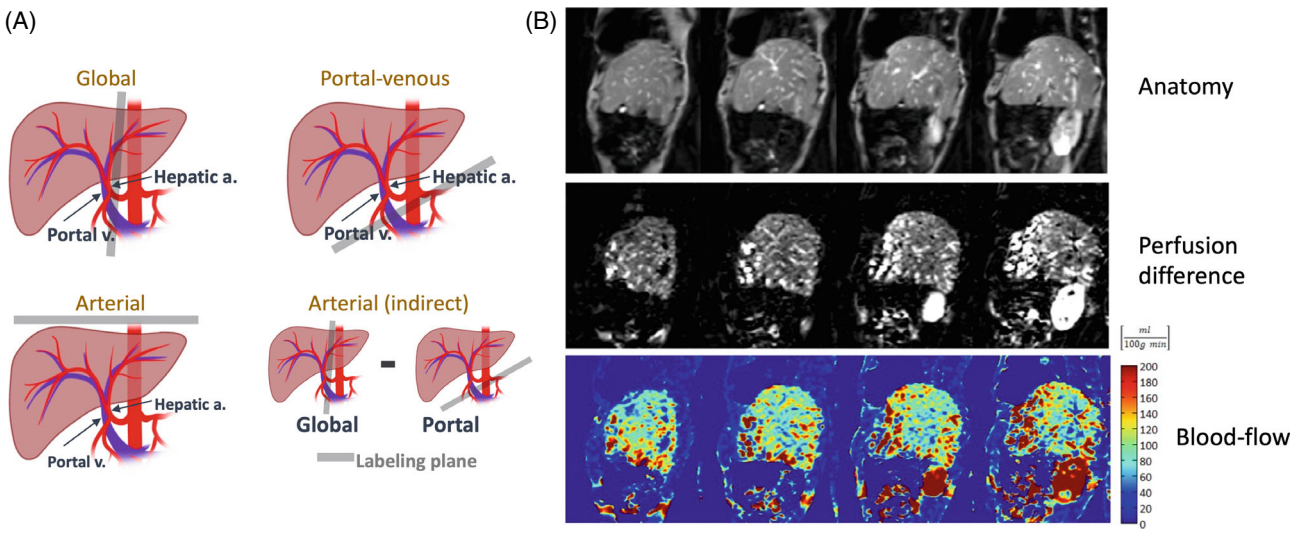

FIGURE 7 (A) Labeling schemes for measuring global, portal-venous, and arterial liver perfusion with a PCASL sequence. (B) Representative anatomical (PD-weighted), perfusion-weighted and quantitative hepatic blood flow images. ASL data were acquired with a background suppressed PCASL-EPI sequence at 3T (2 s labeling/2 s PLD)

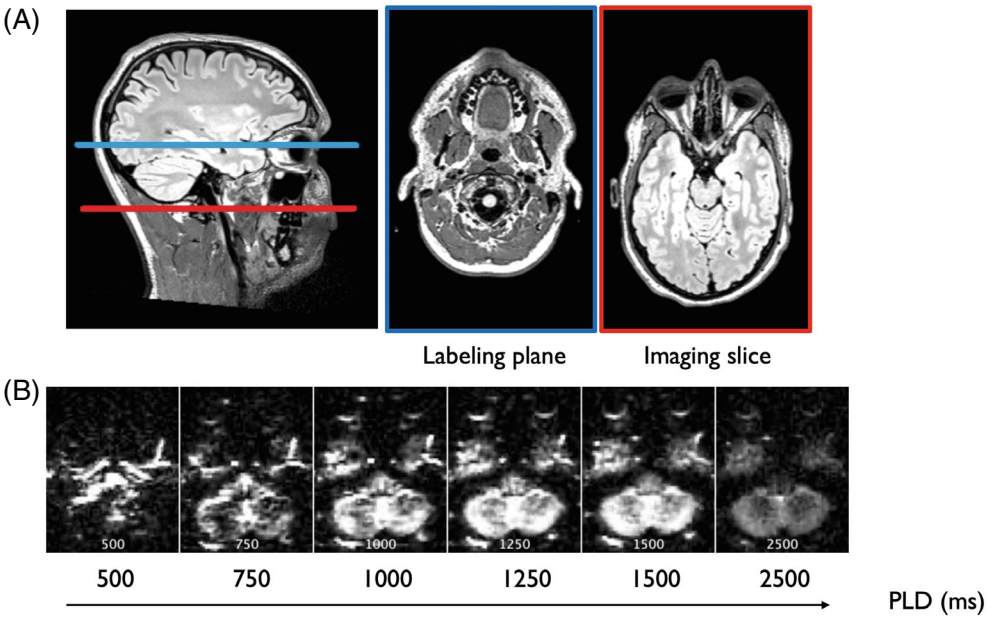

FIGURE 8 (A) Illustration of planning for retinal perfusion imaging with PCASL and single-slice readout. (B) Example of multi-delay PCASL-SSFSE data in the retina (courtesy of D. Alsop)

et al.[103] minimizing motion by eye fixation on a target and synchronizing breathing and eye blinking to the end readout. Using this approach, a marked reduction in retinal blood flow was observed in patients with retinitis pigmentosa, compared with healthy controls.[104] Finally, intra and inter session reproducibility of retinal blood flow values was assessed using PCASL with a 3D-GRASE readout, with thin slices.[105]

3.6.3 | Recommendations

- Both PASL and PCASL labeling strategies are appropriate for retinal ASL.
- The labeling plane should be positioned 5–7 cm below the imaging volume to label blood in the internal carotid arteries.
- A readout sequence with low sensitivity to magnetic field inhomogeneities is recommended. An approximately axial slice orientation is adequate. High in-plane resolution and thin slices are desirable.
- Background suppression is required to minimize motion effects and increase tSNR.
- The use of stable visual fixation during scanning and motion correction during post-processing can also reduce motion artifacts.

3.7 | Pancreas

The pancreas is a unique organ with major endocrine (responsible for producing hormones for blood-sugar control) and exocrine (secretion of digestive enzymes) functions. This explains the numerous conditions in which imaging pancreatic perfusion would be relevant, from diabetes to chronic pancreatitis or pancreatic cancer.

3.7.1 | Challenges

The main challenges related to pancreatic imaging are presence of large air pockets in surrounding bowels leading to strong local susceptibility gradients as well as peristaltic motion, in addition to respiratory motion. In addition, the arterial supply to the pancreas originates from branches of the superior mesenteric artery (SMA) but also from the splenic artery, with different regions of the pancreas (head, body and tail) being supplied by different arteries. Finally, the pancreas has a very short longitudinal relaxation time T_1, measured to be 584 ms at 1.5T and 725 ms at 3T[106] causing very rapid signal decay during the time course of an ASL experiment.

3.7.2 | Developments

Several reports have successfully measured pancreatic blood flow using ASL in healthy volunteers at rest and during stimulation. Using a FAIR-bSSFP sequence at 1.5T, the first reports of pancreatic ASL were published in 2006 and 2008[107,108] in healthy volunteers, reporting initial values for resting pancreatic blood flow that were comparable to CT-perfusion and DCE-derived measurements.[109,110] More recently, Taso et al. used a background-suppressed SSFSE-PCASL at 3 T[111] to take advantage of the longer T_1

for measuring blood flow and transit-time using a sequential multi-delay strategy, reporting an average ATT of 1 s. A representative dataset is shown in Figure 9. Consistency of pancreatic ASL has been assessed in several studies showing good scan-rescan reproducibility.[111–113]

In parallel, several groups designed and executed studies looking at modulation of pancreatic blood flow using either intravenous secretin (a hormone responsible for stimulating pancreatic exocrine secretions) or oral/IV glucose (to stimulate endocrine secretions). In both secretin[112,113] and glucose studies,[111] significant increases in pancreatic perfusion were reported ranging from 16 to 81%. Details are found in Table S4. An important variability can be observed between different studies that can be attributed partially to different technical implementations but also different pancreatic regions scanned (head or tail). However, besides a single study in Type-1 diabetes,[114] no clinical study has been reported using ASL in pancreatic diseases.

3.7.3 | Summary

Although the literature on pancreatic ASL has been sparse, the following can be extracted from up-to-date evidence:

- Both FAIR and PCASL labeling strategies are appropriate and have been successfully used to measure pancreatic blood flow.
- Choice of orientation might depend on the application.
- Longer pancreatic T_1 might favor the use of 3T although successful 1.5T studies have been reported.
- Blood flow quantification using two-compartment models (blood and tissue) is more accurate.
- Subject preparation has to be considered as the pancreas is heavily impacted by peristalsis.
- Background suppression is desirable to minimize physiological motion impact.

3.8 | Muscle

More than any organ, skeletal muscle perfusion varies widely between rest and maximal hyperemic states, increasing from <5 ml/min/100 g at rest[115] to 80 ml/min/100 g or more following exercise.[115–117] In addition, in contrast to many vital organs discussed herein, perfusion to skeletal muscle may be interrupted for minutes to hours without lasting consequences. For instance, a proximal tourniquet may be applied to halt the arterial inflow and create a bloodless surgical field for lower extremity surgery.[118] This resilience of muscle to withstand periods of arterial occlusion opens the door to probe not only the response to exercise but also the dynamic response following induced ischemia as highlighted in Figure 10, somewhat akin to cardiac stress testing or cerebrovascular reactivity measurements, where the temporal

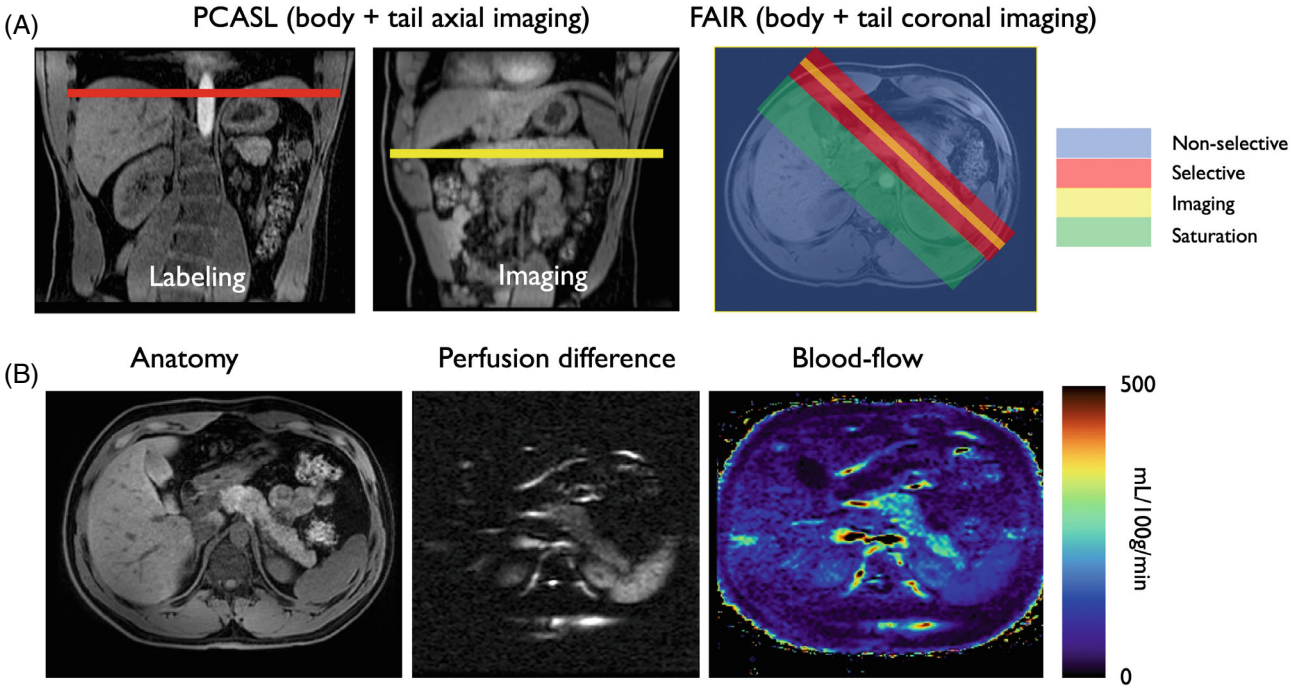

FIGURE 9 (A) Labeling geometry for FAIR and PCASL pancreatic perfusion imaging and (B) illustration of a dataset with anatomical, perfusion-weighted and pancreatic blood-flow in a healthy volunteer acquired using a PCASL-SSFSE sequence at 3T

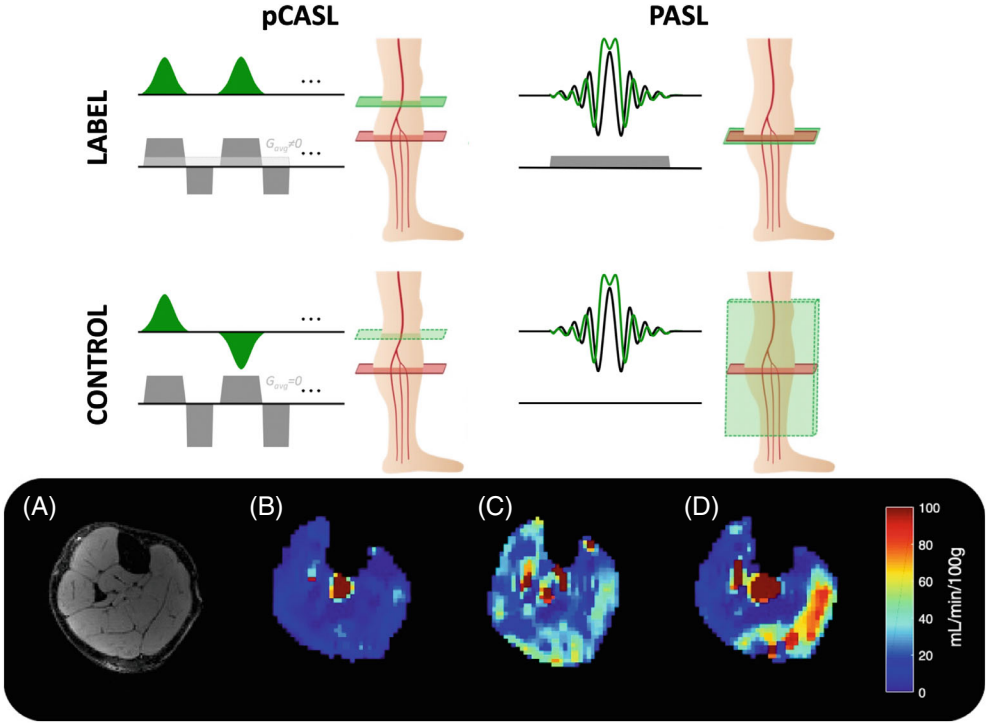

FIGURE 10 Representative anatomical (A) and perfusion images at rest (B), following induced ischemia (C), and after plantar flexion exercise (D) in a healthy participant. Note the global hyperemia observed during reactive hyperemia in C, while only the activated gastrocnemius muscle is hyperperfused in D. ASL data were acquired with vPIVOT, an interleaved PASL, phase contrast, and multi-echo GRE sequence as detailed in Englund et al, Magn Reson Med 2018 (Reference 117)

kinetics of the muscle blood flow response provide insight into endothelial function.[119,120]

3.8.1 | Challenges

Since baseline muscle perfusion is extremely low, it may be under the detection limit of conventional ASL. Furthermore, with the recruitment of collateral arteries, resting perfusion is typically maintained even in mild to moderate disease such as peripheral artery disease and diabetes. Functional deficits in these diseases are revealed when measuring the perfusion response to a vasoactive stimulus[119–123] and therefore methodologically, high temporal resolution is needed to evaluate dynamic responses. For ASL acquisitions which are heavily T2*-weighted, underlying signal changes (e.g., linked to oxygenation) that occur during these vasoactive stimuli can bias the quantified perfusion unless corrected. This signal variation is typically corrected by interpolating the control series to create temporally-matched acquisitions of label and control data,[116,124] or more recently through the use of background suppression.[125]

In contrast to some other organs with straightforward feeding vessels (e.g., brain or kidneys), the muscle blood supply may branch off large arteries at several points while the conduit artery continues past the muscle of interest to distal locations. In addition, while the capillaries are primarily aligned with the long axis of the muscle fiber,[126] the orientation of the feeding vessels with respect to the muscle varies. For example, the lumbar arteries that supply the paraspinal muscles of the low back enter the muscle perpendicularly, while the sural branches of the popliteal artery that supply the gastrocnemius muscle run parallel with the muscle's long axis.

In addition to these geometric differences, there is also variability in the arterial flow waveform between rest and hyperemic states as highlighted in Figure 10. In healthy individuals, resting blood flow in the large arteries supplying skeletal muscle is typically triphasic, with forward flow during systole and retrograde then antegrade flow during diastole.[127] As blood flow increases during exercise or following induced ischemia, the arterial flow profile becomes monophasic (i.e., entirely antegrade).[128] These differences may be important when using ASL methods that rely on flow-driven adiabatic inversion, though relative agreement has been observed when comparing PASL and PCASL-based perfusion measurements.[129]

3.8.2 | Developments

To overcome these obstacles related to slow and recirculating flow and achieve high temporal resolution, many investigators have recently opted for PASL over CASL/PCASL. However, PASL,[116] CASL,[130] PCASL,[123] and VS-ASL[131] have all been employed to evaluate muscle perfusion. Most studies quantified perfusion in muscles of the leg, with notable exceptions in the masseter muscle,[132] as well as muscles of the feet,[133,134] and forearm.[133,135]

From a technical development standpoint, many of the sequences are adapted from those developed for other organs, however analysis strategies focus on the dynamic changes associated with exercise or reactive hyperemia rather than quantification of steady-state perfusion in resting or active state.

There have been a few sequences that were specifically developed to quantify skeletal muscle perfusion, including Flow-driven Arterial Water Stimulation With elimination of Tissue Signal (FAWSETS), a CASL variant that utilizes adiabatic excitation rather than inversion,[136,137] and saturation inversion recovery (SATIR), an adaptation of FAIR employing a saturation pulse to ensure identical initial magnetization in the imaging slice.[116] These sequences, however, are limited to single-slice acquisitions. Recently, Baligand, et al. demonstrated multi-slice perfusion quantification using FAIR with a split-labeling scheme,[125] which may provide insight into the spatial heterogeneity of perfusion along a muscle.

Additional technical developments have focused on acquiring complementary functional parameters, providing a comprehensive evaluation of muscle blood flow, oxygen extraction, and metabolic changes. For example, Duteil et al. used an interleaved ASL, $^{1}H/^{31}P$-MRS sequence to simultaneously measure perfusion, deoxymyoglobin concentration and phosphocreatine resynthesis rate following ischemic exercise.[138] In addition, ASL has been combined with BOLD to evaluate the relationship between relative oxygenation and blood flow changes,[124,139,140] or more recently combined with quantitative oximetry methods such as T2*-,[141,142] T2-[143], or susceptibility-based oximetry,[117,124] for the evaluation of muscle oxygen consumption. One such method, termed vPIVOT uses an interleaved ASL, multi-echo GRE, and phase contrast acquisition strategy to simultaneously quantify perfusion, bulk arterial/venous blood flow, venous oxygen saturation in a large draining vein, and relative T2* changes, together yielding a comprehensive sequence to evaluate micro- and macro-vascular blood flow and oxygenation responses in muscle.[117] Muscle ASL studies to date are summarized in Table S5 and an example dataset is shown in Figure 10.

3.8.3 | Summary

Based on previous studies of ASL in skeletal muscle, we can summarize the following:

- Quantification of muscle perfusion is possible with both PASL and PCASL methods, however PASL yields higher temporal resolution which may be desirable for measuring the response kinetics.
- Muscle perfusion at rest is extremely low and largely preserved in pathologic states, therefore most studies evaluated the perfusion dynamics following a vasoactive stimulus (e.g., exercise or induced ischemia).
- When quantifying time-resolved perfusion, correction of underlying T2*-weighted signal intensity changes must be performed, either requiring temporal matching of tag and control images or efficient background suppression.

3.9 | Other regions

In addition to the regions mentioned above, it is worth mentioning that several other clinically important regions have been explored with ASL, including the spinal cord,[144] thyroid gland,[145] spleen,[93,146,147] prostate,[148] and reproductive organs.[149]

3.10 | ASL validation against reference methods

Although critical, validation of blood flow measurements with ASL in human subjects are challenging especially in the body where gold-standard reference methods are usually not well established. While several studies cited in specific sections have performed correlation analyses of ASL with other methods sensitive to perfusion such as DCE or CT-perfusion, validation against methods referred to as gold standards such as $[^{15}O]$-H_2O-PET or microsphere counting are scarce. Of interest, a few animal studies have compared ASL blood flow quantification to fluorescent microspheres demonstrating very good correlations between ASL and microspheres for kidney[150] and myocardial blood flow measurements.[151]

4 | FUTURE DEVELOPMENTS FOR WIDER AVAILABILITY AND ROBUSTNESS OF BODY ASL: WHAT IS NEXT?

4.1 | Toward standardized body ASL implementations

Initial ASL experiments in some abdominal and thoracic body organs were carried out soon after the first brain ASL studies.[3,71] However, as already mentioned, body ASL methods have until recently evolved at a slower pace than brain ASL. In some organs (especially kidney), the amount of accumulated data is substantial and shows that these techniques have great potential for clinical application.

However, efforts must be made to standardize implementations and processing methods and to assess and improve measurement reproducibility in order to push ASL use into clinical trials and ultimately routine practice.

For renal imaging, RENALMRI.org* is a multidisciplinary network of clinical and basic scientists, stemming from the PARENCHIMA project (funded as a European COST action between 2017 and 2021, footnote 1) which aimed to eliminate barriers to the clinical translation of functional renal MRI techniques, including ASL. PARENCHIMA's efforts translated into a comprehensive review paper highlighting the potential of renal ASL for clinical applications[18] and into a consensus paper on technical recommendations for clinical use[26] as a first step toward standardization. Those recommendations have already been implemented in a project carried out in the United Kingdom, **UKRIN-MAPS** (**UK R**enal **I**maging **N**etwork - **M**RI **A**cquisition and **P**rocessing **Standardization**), which was funded in 2018 by the UK Medical Research Council to develop and validate a comprehensive optimized and harmonized acquisition protocol and data analysis pipelines for multiparametric renal MRI. Following the guidelines proposed in the PARENCHIMA consensus renal ASL paper,[26] harmonized ASL sequences have been implemented on various vendor platforms (GE, Philips, and Siemens), and are currently being tested and compared in healthy subjects through a multi-site traveling volunteer study. It is worth noting that ASL is also a focus of the Quantitative Imaging Network (QIN), which is a consortium of research groups with funded grants from the National Cancer Institute (NCI) of the United States' National Institutes of Health (NIH).[132] The QIN promotes research, development, and validation of quantitative imaging tools for the measurement or prediction of tumor response to therapies in clinical trial settings. In addition, QIN also facilitates collaborative projects for testing protocols and processing algorithms across platforms and sites. These efforts will facilitate the transition of ASL as an imaging biomarker into clinical settings.

4.2 | Perspectives at high- and/or low-field for body ASL

The choice of field strength for body ASL is an important one. Reasons for higher field (>3T) are increased magnetization[152] and longer T_1 relaxation times,[153] both of which provide a stronger ASL signal. However, this also brings technical issues, such as stronger off-resonance effects (including susceptibility-related signal loss, artifacts, and image distortion), B_1^+ variation, and SAR limits. Lower field strength (<1.5T) provides lower ASL signal but substantially fewer artifacts, and increased flexibility in the design of the ASL experiment. Researchers are also limited by what equipment is accessible, with 1.5T and 3T being the dominant whole-body platforms worldwide at this time. Ultimately when choosing a field strength for body ASL, one must consider the temporal SNR efficiency that will be achieved.

Most body ASL studies discussed have been performed on clinical scanners (≤3T). Recently 7T ASL has drawn much attention in the brain, and some studies have demonstrated the feasibility to acquire high spatial resolution ASL.[154,155] 7 T can also benefit body ASL in several aspects. For example, image acquisition times can be reduced and motion-associated artifacts minimized due to increased SNR and potentially better parallel imaging performance.[156] Li et al. demonstrated the feasibility of single breath-hold renal ASL at 7T with multiple strategies to address both B_0/B_1 and SAR challenges.[157] 7 T may also be suited to ASL studies in low blood flow organs such as knee bone marrow[158] and skeletal muscle.[140,159] PASL is currently the most popular strategy at 7 T, due to its lower SAR compared to PCASL. It is worth noting that specific RF pulses[160] and/or array coil designs[161] are necessary to improve transmit efficiency, field homogeneity, and SAR performance at 7T.

At the other extreme, Martirosian et al. demonstrated the feasibility of lung perfusion imaging using FAIR ASL at 0.2T, where results showed less signal dropout compared to images acquired at 1.5T.[162] ASL may also be used to monitor blood flow during MR guided therapy, such as RF ablation of renal cell carcinoma, on interventional low field scanners.[163] Recently, Campbell-Washburn et al. proposed a high-performance low-field (0.55T) MR scanner with strong gradient system to compensate for the intrinsic reduced SNR, and demonstrated that high quality lung perfusion imaging can be obtained with minimal distortion.[164]

4.3 | Increasing role of AI/ML

The use of artificial intelligence (AI) in computer vision and medical imaging has exploded in recent years, with a wide range of powerful applications in MRI. From data sampling to image reconstruction, artifact correction, and segmentation, AI is bringing a paradigm shift to medical imaging, and body ASL is no exception.

AI and machine learning (ML) methods, especially deep-learning, have shown excellent potential for improving body ASL, facilitating free-breathing or volumetric imaging, and automating downstream quantitative analysis. For renal imaging, unrolled deep-learning networks have shown the potential for reconstructing heavily undersampled 3D volumes acquired with a variable-density FSE

sequence up to 14-fold acceleration, leading to effective scan times of under 1 min.[165] In cardiac ASL, segmentation of the left ventricular myocardium has always been an incredibly challenging problem, due to the variations in contrast between labeled control and baseline images, and the presence of a large spurious ASL signal in the ventricular blood pool on one side and epicardial fat on the other side. AI/ML methods have provided an efficient solution for segmenting the myocardium,[166,167] and also providing estimates of uncertainty in resulting perfusion maps.[81]

The use of AI/ML can also be expected to improve body ASL spatio-temporal resolution, through undersampled acquisitions, once the research community has accumulated sufficient training data or with the development of AI/ML methods that are less dependent on large dataset sizes. More general use of deep-learning in ASL for reconstruction, denoising or parameter quantification is extensively described in the recently published review on advanced ASL techniques.[168]

5 | CONCLUSIONS

Applications of ASL in the body have blossomed in recent years, approaching institutional standard-of-care for example in renal imaging. From basic developments to clinical applications in specific pathologies, ASL is now a technique capable of imaging perfusion from head to toe. While implementations vary greatly based on specific organ requirements especially with regards to labeling schemes, this group of experts consider that the following are consistent features to consider when implementing body ASL methods:

- Background-suppression is desirable for body applications and is potentially enabling in some cases.
- Both 1.5T and 3T field strengths are appropriate. While 3T offers higher intrinsic SNR, reduced dielectric and susceptibility effects might favor 1.5T for some applications.
- Motion mitigation strategies are often critical. The choice between prospective, retrospective, and a combination of both depends on the target organ and sequence implementation.

Finally, as is already underway in the renal imaging field, large initiatives for reproducible, standardized imaging as well as validation strategies are key in facilitating wide deployment and adoption of ASL for contrast-free, quantitative body perfusion imaging.

AFFILIATIONS

[1]Division of MRI Research, Department of Radiology, Beth Israel Deaconess Medical Center and Harvard Medical School, Boston, Massachusetts, USA

[2]Department of Radiology, Clínica Universidad de Navarra, Pamplona, Spain

[3]Department of Radiology, University of Colorado Anschutz Medical Campus, Aurora, Colorado, USA

[4]Sir Peter Mansfield Imaging Center, University of Nottingham, Nottingham, UK

[5]C.J. Gorter Center for High Field MRI, Department of Radiology, Leiden University Medical Center, Leiden, The Netherlands

[6]Center for Image Sciences, University Medical Centre Utrecht, Utrecht, The Netherlands

[7]Department of Radiology, Advanced Imaging Research Center, and Biomedical Engineering, UT Southwestern Medical Center, Dallas, Texas, USA

[8]Section on Experimental Radiology, Department of Radiology, University Hospital of Tuebingen, Tuebingen, Germany

[9]Ming Hsieh Department of Electrical and Computer Engineering, University of Southern California, Los Angeles, California, USA

[10]The Russell H. Morgan Department of Radiology and Radiological Science, Johns Hopkins University, Baltimore, Maryland, USA

[11]Laboratory of FMRI Technology (LOFT), Mark & Mary Stevens Neuroimaging and Informatics Institute, Keck School of Medicine, University of Southern California, Los Angeles, California, USA

[12]Department of Brain Repair and Rehabilitation, UCL Queen Square Institute of Neurology, University College London, London, UK

[13]Department of Radiology, Weill Cornell Medicine, New York, New York, USA

ACKNOWLEDGMENTS

The work in this article has been endorsed by the ISMRM perfusion study section and by the ISMRM's board of trustees. Endorsement was obtained by a survey among the perfusion study group's members and by subsequent endorsement by the board of trustees. ZZ is supported by the NIH/NICHD grant R01HD100012. MFS and VAV acknowledge support from ERAPERMED2020-326-RESPECT, PC181-182 RM-RENAL and PI21/00578. DLT is supported by the UCLH NIHR Biomedical Research Centre and the Wellcome Trust (Centre award 539208). AJM acknowledges the support from NIH/NCI U01CA207091. EKE is supported by NIH/NCATS Colorado CTSA Grant Number UL1 TR002535 and KL2 TR002534, and AHA853697. QQ is supported by the NIH/NHLBI grants R01HL138182 and R01HL144751.

ENDNOTE

*https://www.cost.eu/actions/CA16103

ORCID

Manuel Taso https://orcid.org/0000-0003-2405-9165
Veronica Aramendía-Vidaurreta https://orcid.org/0000-0001-9834-2866
Suzanne Franklin https://orcid.org/0000-0001-6886-5578
Ananth J. Madhuranthakam https://orcid.org/0000-0002-5524-7962
Krishna S. Nayak https://orcid.org/0000-0001-5735-3550
Qin Qin https://orcid.org/0000-0002-6432-2944
Xingfeng Shao https://orcid.org/0000-0002-4130-6204
David L. Thomas https://orcid.org/0000-0003-1491-1641
Zungho Zun https://orcid.org/0000-0002-7297-3990

TWITTER

Manuel Taso @ManuelTaso

REFERENCES

1. Detre JA, Zhang W, Roberts DA, et al. Tissue specific perfusion imaging using arterial spin labeling. *NMR Biomed*. 1994;7:75-82.
2. Williams DS, Detre JA, Leigh JS, Koretsky AP. Magnetic resonance imaging of perfusion using spin inversion of arterial water. *Proc Natl Acad Sci U S A*. 1992;89:212-216.
3. Roberts DA, Detre JA, Bolinger L, et al. Renal perfusion in humans: MR imaging with spin tagging of arterial water. *Radiology*. 1995;196:281-286.
4. Alsop DC, Detre JA, Golay X, et al. Recommended implementation of arterial spin labeled perfusion MRI for clinical applications: a consensus of the ISMRM perfusion study group and the European consortium for ASL in dementia. *Magn Reson Med*. 2015;73:102-116.
5. McDonald RJ, Levine D, Weinreb J, et al. Gadolinium retention: a research roadmap from the 2018 NIH/ACR/RSNA workshop on gadolinium chelates. *Radiology*. 2018;289:517-534.
6. Brandner ED, Wu A, Chen H, et al. Abdominal organ motion measured using 4D CT. *Int J Radiat Oncol Biol Phys*. 2006;65:554-560.
7. Shin T, Worters PW, Hu BS, Nishimura DG. Non-contrast-enhanced renal and abdominal MR angiography using velocity-selective inversion preparation. *Magn Reson Med*. 2013;69:1268-1275.
8. Zhu D, Li W, Liu D, et al. Non-contrast-enhanced abdominal MRA at 3 T using velocity-selective pulse trains. *Magn Reson Med*. 2020;84:1173-1183.
9. Hashimoto J, Ito S. Aortic stiffness determines diastolic blood flow reversal in the descending thoracic aorta. *Hypertension*. 2013;62:542-549.
10. Verbree J, van Osch MJP. Influence of the cardiac cycle on pCASL: cardiac triggering of the end-of-labeling. *Magn Reson Mater Phys Biol Med*. 2018;31:223-233.
11. Bergin CJ, Glover GH, Pauly JM. Lung parenchyma: magnetic susceptibility in MR imaging. *Radiology*. 1991;180:845-848.
12. Verma T, Cohen-Adad J. Effect of respiration on the B0 field in the human spinal cord at 3T. *Magn Reson Med*. 2014;72:1629-1636.
13. Bernstein MA, Huston J, Ward HA. Imaging artifacts at 3.0 T. *J Magn Reson Imaging*. 2006;24:735-746.
14. Merkle EM, Dale BM. Abdominal MRI at 3.0 T: the basics revisited. *Am J Roentgenol*. 2006;186:1524-1532.
15. Sung K, Nayak KS. Design and use of tailored hard-pulse trains for uniformed saturation of myocardium at 3 tesla. *Magn Reson Med*. 2008;60:997-1002.
16. Franklin SL, Bones IK, Harteveld AA, et al. Multi-organ comparison of flow-based arterial spin labeling techniques: spatially non-selective labeling for cerebral and renal perfusion imaging. *Magn Reson Med*. 2021;85:2580-2594.
17. Xu F, Li W, Liu D, et al. A novel spectrally selective fat saturation pulse design with robustness to B0 and B1 inhomogeneities: a demonstration on 3D T1-weighted breast MRI at 3 T. *Magn Reson Imaging*. 2021;75:156-161.
18. Odudu A, Nery F, Harteveld AA, et al. Arterial spin labelling MRI to measure renal perfusion: a systematic review and statement paper. *Nephrol Dial Transplant*. 2018;33:ii15-ii21.
19. Stevens LA, Coresh J, Greene T, Levey AS. Assessing kidney function--measured and estimated glomerular filtration rate. *N Engl J Med*. 2006;354:2473-2483.
20. Webster AC, Nagler EV, Morton RL, Masson P. Chronic kidney disease. *Lancet*. 2017;389:1238-1252.
21. Fraum TJ, Ludwig DR, Bashir MR, Fowler KJ. Gadolinium-based contrast agents: a comprehensive risk assessment. *J Magn Reson Imaging*. 2017;46:338-353.
22. Echeverria-Chasco R, Vidorreta M, Aramendía-Vidaurreta V, et al. Optimization of pseudo-continuous arterial spin labeling for renal perfusion imaging. *Magn Reson Med*. 2021;85:1507-1521.
23. Schwartz LH, Richaud J, Buffat L, Touboul E, Schlienger M. Kidney mobility during respiration. *Radiother Oncol*. 1994;32:84-86.
24. Becker AS, Rossi C. Renal arterial spin labeling magnetic resonance imaging. *Nephron*. 2017;135:1-5.
25. Nery F, Gordon I, Thomas D. Non-invasive renal perfusion imaging using arterial spin labeling MRI: challenges and opportunities. *Diagnostics*. 2018;8:2.
26. Nery F, Buchanan CE, Harteveld AA, et al. Consensus-based technical recommendations for clinical translation of renal ASL MRI. *Magn Reson Mater Phys Biol Med*. 2020;33:141-161.
27. Zhou L, Wang Y, Madhuranthakam A. Improving the robustness of pseudo-continuous arterial spin labeling for renal perfusion imaging. *Proceedings of the 2021 ISMRM Annual Meeting*. Virtual; 2021:2539.
28. Harteveld AA, de Boer A, Franklin SL, Leiner T, van Stralen M, Bos C. Comparison of multi-delay FAIR and pCASL labeling approaches for renal perfusion quantification at 3T MRI. *Magn Reson Mater Phys Biol Med*. 2020;33:81-94.
29. Lu F, Yang J, Yang S, et al. Use of three-dimensional arterial spin labeling to evaluate renal perfusion in patients with chronic kidney disease. *J Magn Reson Imaging*. 2021;54:1152-1163.
30. Bones IK, Franklin SL, Harteveld AA, et al. Influence of labeling parameters and respiratory motion on velocity-selective arterial spin labeling for renal perfusion imaging. *Magn Reson Med*. 2020;84:1919-1932.

31. Bones IK, Franklin SL, Harteveld AA, et al. Exploring label dynamics of velocity-selective arterial spin labeling in the kidney. *Magn Reson Med*. 2021;86:131-142.
32. Qin Q, van Zijl PCM. Velocity-selective-inversion prepared arterial spin labeling. *Magn Reson Med*. 2016;76:1136-1148.
33. Liu D, Li W, Xu F, Zhu D, Shin T, Qin Q. Ensuring both velocity and spatial responses robust to B 0 / B 1 + field inhomogeneities for velocity-selective arterial spin labeling through dynamic phase-cycling. *Magn Reson Med*. 2021;85:2723-2734.
34. Landes V, Javed A, Jao T, Qin Q, Nayak K. Improved velocity-selective labeling pulses for myocardial ASL. *Magn Reson Med*. 2020;84:1909-1918.
35. Nery F, De Vita E, Clark CA, Gordon I, Thomas DL. Robust kidney perfusion mapping in pediatric chronic kidney disease using single-shot 3D-GRASE ASL with optimized retrospective motion correction. *Magn Reson Med*. 2018;81:2972-2984.
36. Greer JS, Wang X, Wang Y, et al. Robust pCASL perfusion imaging using a 3D Cartesian acquisition with spiral profile reordering (CASPR). *Magn Reson Med*. 2019;82:1713-1724.
37. Taso M, Zhao L, Guidon A, Litwiller DV, Alsop DC. Volumetric abdominal perfusion measurement using a pseudo-randomly sampled 3D fast-spin-echo (FSE) arterial spin labeling (ASL) sequence and compressed sensing reconstruction. *Magn Reson Med*. 2019;82:680-692.
38. Cutajar M, Thomas DL, Banks T, Clark CA, Golay X, Gordon I. Repeatability of renal arterial spin labelling MRI in healthy subjects. *Magma N Y N*. 2012;25:145-153.
39. Ning Z, Chen S, Chen Z, et al. Saturated multi-delay renal arterial spin labeling technique for simultaneous perfusion and T1 quantification in kidneys. *Magn Reson Med*. 2022;88:1055-1067.
40. Henderson AC, Prisk GK, Levin DL, Hopkins SR, Buxton RB. Characterizing pulmonary blood flow distribution measured using arterial spin labeling. *NMR Biomed*. 2009;22:1025-1035.
41. Schraml C, Schwenzer NF, Martirosian P, et al. Non-invasive pulmonary perfusion assessment in young patients with cystic fibrosis using an arterial spin labeling MR technique at 1.5 T. *Magma*. 2012;25:155-162.
42. Greer JS, Maroules CD, Oz OK, et al. Non-contrast quantitative pulmonary perfusion using flow alternating inversion recovery at 3T: a preliminary study. *Magn Reson Imaging*. 2018;46:106-113.
43. Greer JS, Michael J, Burkhardt B, et al. Caval blood flow distribution in Fontan circulation: comparison between ASL-measured pulmonary perfusion and 4D flow. *Proceedings of the Joint Annual Meeting ISMRM-ESMRMB*. Vol 26. Paris, France; 2018:4.
44. Seith F, Pohmann R, Schwartz M, et al. Imaging pulmonary blood flow using Pseudocontinuous arterial spin labeling (PCASL) with balanced steady-state free-precession (bSSFP) readout at 1.5 T. *J Magn Reson Imaging*. 2020;52:1767-1782.
45. Greer JS, Wang Y, Zhou L, Hussain T, Madhuranthakam AJ. Robust non-contrast pulmonary perfusion imaging using pseudo-continuous arterial spin labeling with background suppression. *Proceedings of the 28th Annual Meeting of ISMRM*. Vol 28. Virtual; 2020:3277.
46. Greer JS, Gooty V, Tandon A, Greil G, Hussain T, Madhuranthakam AJ. Non-contrast, free-breathing pulmonary perfusion imaging in pediatric patients with congenital heart disease using multi-slice FAIR at 1.5T. *Proceedings of the 27th annual ISMRM meeting, Montreal*. QC, Canada; 2019:2175.
47. Greer JS, Abdulkareem M, Greil GF, Zia A, Madhuranthakam AJ, Hussain T. Quantification of arterial obstruction in pediatric patients with pulmonary embolism using arterial spin labeled perfusion MRI of the lungs. *Proceedings of the 29th Annual Meeting of ISMRM*. Vol 29. Virtual; 2021:476.
48. Burton GJ, Woods AW, Jauniaux E, Kingdom JCP. Rheological and physiological consequences of conversion of the maternal spiral arteries for Uteroplacental blood flow during human pregnancy. *Placenta*. 2009;30:473-482.
49. Bucklin B, Baysinger C, Gambling D. *A Practical Approach to Obstetric Anesthesia*. Second ed. LWW; 2016.
50. Shao X, Liu D, Martin T, et al. Measuring human placental blood flow with multidelay 3D GRASE pseudocontinuous arterial spin labeling at 3T. *J Magn Reson Imaging*. 2018;47:1667-1676.
51. Gowland PA, Francis ST, Duncan KR, et al. In vivo perfusion measurements in the human placenta using echo planar imaging at 0.5 T. *Magn Reson Med*. 1998;40:467-473.
52. Guttmacher AE, Maddox YT, Spong CY. The human placenta project: placental structure, development, and function in real time. *Placenta*. 2014;35:303-304.
53. Derwig I, Lythgoe DJ, Barker GJ, et al. Association of placental perfusion, as assessed by magnetic resonance imaging and uterine artery Doppler ultrasound, and its relationship to pregnancy outcome. *Placenta*. 2013;34:885-891.
54. Zun Z, Zaharchuk G, Andescavage NN, Donofrio MT, Limperopoulos C. Non-invasive placental perfusion imaging in pregnancies complicated by fetal heart disease using velocity-selective arterial spin labeled MRI. *Sci Rep*. 2017;7:16126.
55. Zun Z, Limperopoulos C. Placental perfusion imaging using velocity-selective arterial spin labeling. *Magn Reson Med*. 2018;80:1036-1047.
56. Ludwig KD, Fain SB, Nguyen SM, et al. Perfusion of the placenta assessed using arterial spin labeling and ferumoxytol dynamic contrast enhanced magnetic resonance imaging in the rhesus macaque. *Magn Reson Med*. 2019;81:1964-1978.
57. Hutter J, Harteveld AA, Jackson LH, et al. Perfusion and apparent oxygenation in the human placenta (PERFOX). *Magn Reson Med*. 2020;83:549-560.
58. Harteveld AA, Hutter J, Franklin SL, et al. Systematic evaluation of velocity-selective arterial spin labeling settings for placental perfusion measurement. *Magn Reson Med*. 2020;84:1828-1843.
59. Liu D, Shao X, Danyalov A, et al. Human placenta blood flow during early gestation with Pseudocontinuous arterial spin labeling MRI. *J Magn Reson Imaging*. 2020;51:1247-1257.
60. Heart Disease and Stroke Statistics—2020 Update: A Report From the American Heart Association | Circulation. 10.1161/CIR.0000000000000757. Accessed April 12, 2021.
61. Nichols M, Townsend N, Scarborough P, Rayner M. Cardiovascular disease in Europe: epidemiological update. *Eur Heart J*. 2013;34:3028-3034.
62. Gould KL, Lipscomb K. Effects of coronary stenoses on coronary flow reserve and resistance. *Am J Cardiol*. 1974;34:48-55.
63. Kober F, Jao T, Troalen T, Nayak KS. Myocardial arterial spin labeling. *J Cardiovasc Magn Reson*. 2016;18:22.

64. Buxton RB, Frank LR, Wong EC, Siewert B, Warach S, Edelman RR. A general kinetic model for quantitative perfusion imaging with arterial spin labeling. *Magn Reson Med*. 1998;40:383-396.
65. Detre JA, Leigh JS, Williams DS, Koretsky AP. Perfusion imaging. *Magn Reson Med*. 1992;23:37-45.
66. Zun Z, Wong EC, Nayak KS. Assessment of myocardial blood flow (MBF) in humans using arterial spin labeling (ASL): feasibility and noise analysis. *Magn Reson Med*. 2009;62:975-983.
67. Zun Z, Varadarajan P, Pai RG, Wong EC, Nayak KS. Arterial spin labeled CMR detects clinically relevant increase in myocardial blood flow with vasodilation. *JACC Cardiovasc Imaging*. 2011;4:1253-1261.
68. Yoon AJ, Do HP, Cen S, et al. Assessment of segmental myocardial blood flow and myocardial perfusion reserve by adenosine-stress myocardial arterial spin labeling perfusion imaging. *J Magn Reson Imaging JMRI*. 2017;46:413-420.
69. Aramendía-Vidaurreta V, García-Osés A, Vidorreta M, Bastarrika G, Fernández-Seara MA. Optimal repetition time for free breathing myocardial arterial spin labeling. *NMR Biomed*. 2019;32:e4077.
70. Aramendía-Vidaurreta V, Echeverría-Chasco R, Vidorreta M, Bastarrika G, Fernández-Seara MA. Quantification of myocardial perfusion with vasodilation using arterial spin labeling at 1.5T. *J Magn Reson Imaging JMRI*. 2021;53:777-788.
71. Poncelet BP, Koelling TM, Schmidt CJ, et al. Measurement of human myocardial perfusion by double-gated flow alternating inversion recovery EPI. *Magn Reson Med*. 1999;41:510-519.
72. Do HP, Yoon AJ, Fong MW, Saremi F, Barr ML, Nayak KS. Double-gated myocardial ASL perfusion imaging is robust to heart rate variation. *Magn Reson Med*. 2017;77:1975-1980.
73. Javed A, Nayak KS. Single-shot EPI for ASL-CMR. *Magn Reson Med*. 2020;84:738-750.
74. Henningsson M, Carlhäll C-J, Kihlberg J. Myocardial arterial spin labeling in systole and diastole using flow-sensitive alternating inversion recovery with parallel imaging and compressed sensing. *NMR Biomed*. 2021;34:e4436.
75. Wacker CM, Bock M, Hartlep AW, et al. Changes in myocardial oxygenation and perfusion under pharmacological stress with dipyridamole: assessment using T*2 and T1 measurements. *Magn Reson Med*. 1999;41:686-695.
76. Wacker CM, Fidler F, Dueren C, et al. Quantitative assessment of myocardial perfusion with a spin-labeling technique: preliminary results in patients with coronary artery disease. *J Magn Reson Imaging JMRI*. 2003;18:555-560.
77. Wang DJJ, Bi X, Avants BB, Meng T, Zuehlsdorff S, Detre JA. Estimation of perfusion and arterial transit time in myocardium using free-breathing myocardial arterial spin labeling with navigator-echo. *Magn Reson Med*. 2010;64:1289-1295.
78. Keith GA, Rodgers CT, Chappell MA, Robson MD. A look-locker acquisition scheme for quantitative myocardial perfusion imaging with FAIR arterial spin labeling in humans at 3 tesla. *Magn Reson Med*. 2017;78:541-549.
79. Do HP, Jao TR, Nayak KS. Myocardial arterial spin labeling perfusion imaging with improved sensitivity. *J Cardiovasc Magn Reson*. 2014;16:15.
80. Aramendía-Vidaurreta V, Gordaliza PM, Vidorreta M, et al. Reduction of motion effects in myocardial arterial spin labeling. *Magn Reson Med*. 2022;87:1261-1275.
81. Do HP, Guo Y, Yoon AJ, Nayak KS. Accuracy, uncertainty, and adaptability of automatic myocardial ASL segmentation using deep CNN. *Magn Reson Med*. 2020;83:1863-1874.
82. Chareonthaitawee P, Kaufmann PA, Rimoldi O, Camici PG. Heterogeneity of resting and hyperemic myocardial blood flow in healthy humans. *Cardiovasc Res*. 2001;50:151-161.
83. Northrup BE, McCommis KS, Zhang H, et al. Resting myocardial perfusion quantification with CMR arterial spin labeling at 1.5 T and 3.0 T. *J Cardiovasc Magn Reson*. 2008;10:53.
84. Fidler F, Wacker CM, Dueren C, et al. Myocardial perfusion measurements by spin-labeling under different vasodynamic states. *J Cardiovasc Magn Reson*. 2004;6:509-516.
85. Capron T, Troalen T, Robert B, Jacquier A, Bernard M, Kober F. Myocardial perfusion assessment in humans using steady-pulsed arterial spin labeling. *Magn Reson Med*. 2015;74:990-998.
86. Jao TR, Nayak KS. Demonstration of velocity selective myocardial arterial spin labeling perfusion imaging in humans. *Magn Reson Med*. 2018;80:272-278.
87. Noussios G, Dimitriou I, Chatzis I, Katsourakis A. The Main anatomic variations of the hepatic artery and their importance in surgical practice: review of the literature. *J Clin Med Res*. 2017;9:248-252.
88. Sureka B, Patidar Y, Bansal K, Rajesh S, Agrawal N, Arora A. Portal vein variations in 1000 patients: surgical and radiological importance. *Br J Radiol*. 2015;88:20150326.
89. Zoli M, Iervese T, Abbati S, Bianchi GP, Marchesini G, Pisi E. Portal blood velocity and flow in aging man. *Gerontology*. 1989;35:61-65.
90. Chouhan MD, Lythgoe MF, Mookerjee RP, Taylor SA. Vascular assessment of liver disease—towards a new frontier in MRI. *Br J Radiol*. 2016;89:20150675.
91. Gach HM, Li T, Lopez-Talavera JC, Kam AW. Liver perfusion MRI using arterial spin labeling. *Proceedings of the 10th ISMRM Annual Meeting*. Honolulu, HI, USA; 2002:1939.
92. Hoad C, Costigan C, Marciani L, et al. Quantifying blood flow and perfusion in liver tissue using phase contrast angiography and arterial spin labeling. *Proceedings of the 19th ISMRM Annual Meeting*. Montreal, QC, Canada; 2011:794.
93. Bradley CR, Cox EF, Scott RA, et al. Multi-organ assessment of compensated cirrhosis patients using quantitative magnetic resonance imaging. *J Hepatol*. 2018;69:1015-1024.
94. Palaniyappan N, Cox E, Bradley C, et al. Non-invasive assessment of portal hypertension using quantitative magnetic resonance imaging. *J Hepatol*. 2016;65:1131-1139.
95. Cox EF, Palaniyappan N, Aithal GP, Guha IN, Francis ST. Using MRI to study the alterations in liver blood flow, perfusion, and oxygenation in response to physiological stress challenges: meal, hyperoxia, and hypercapnia. *J Magn Reson Imaging*. 2019;49:1577-1586.
96. Katada Y, Shukuya T, Kawashima M, et al. A comparative study between arterial spin labeling and CT perfusion methods on hepatic portal venous flow. *Jpn J Radiol*. 2012;30:863-869.
97. Schalkx HJ, Petersen ET, Peters NHGM, et al. Arterial and portal venous liver perfusion using selective spin labelling MRI. *Eur Radiol*. 2015;25:1529-1540.
98. Pan X, Qian T, Fernandez-Seara MA, et al. Quantification of liver perfusion using multidelay pseudocontinuous arterial spin labeling. *J Magn Reson Imaging*. 2016;43:1046-1054.

99. Martirosian P, Pohmann R, Schraml C, et al. Spatial-temporal perfusion patterns of the human liver assessed by pseudo-continuous arterial spin labeling MRI. *Z Für Med Phys*. 2019;29:173-183.
100. Alsop DC, Maldjian JA, Detre JA. In-Vivo MR perfusion imaging of the human retina. *Proceedings of the 8th ISMRM Annual Meeting*. Denver, CO, USA; 2000:162.
101. Maleki N, Dai W, Alsop DC. Blood flow quantification of the human retina with MRI. *NMR Biomed*. 2011;24:104-111.
102. Maleki N, Alsop DC, Dai W, et al. The effect of hypercarbia and Hyperoxia on the Total blood flow to the retina as assessed by magnetic resonance imaging. *Invest Ophthalmol Vis Sci*. 2011;52:6867-6874.
103. Peng Q, Zhang Y, Nateras OSE, van Osch MJP, Duong TQ. MRI of blood flow of the human retina. *Magn Reson Med*. 2011;65:1768-1775.
104. Zhang Y, Harrison JM, Nateras OSE, Chalfin S, Duong TQ. Decreased retinal–choroidal blood flow in retinitis pigmentosa as measured by MRI. *Doc Ophthalmol*. 2013;126:187-197.
105. Khanal S, Turnbull PRK, Vaghefi E, Phillips JR. Repeatability of arterial spin labeling MRI in measuring blood perfusion in the human eye. *J Magn Reson Imaging*. 2019;49:966-974.
106. de Bazelaire CMJ, Duhamel GD, Rofsky NM, Alsop DC. MR imaging relaxation times of abdominal and pelvic tissues measured in vivo at 3.0 T: preliminary results. *Radiology*. 2004;230:652-659.
107. Qiu M, Wang J, Pinus A, Kim H, Constable RT. Arterial spin labeling TrueFISP pancreas/liver perfusion imaging at 1.5 tesla. *Proceedings of the 14th ISMRM Annual Meeting*. Seattle, WA, USA; 2006:3248.
108. Schraml C, Schwenzer NF, Martirosian P, Claussen CD, Schick F. Perfusion imaging of the pancreas using an arterial spin labeling technique. *J Magn Reson Imaging JMRI*. 2008;28:1459-1465.
109. Coenegrachts K, Van Steenbergen W, De Keyzer F, et al. Dynamic contrast-enhanced MRI of the pancreas: initial results in healthy volunteers and patients with chronic pancreatitis. *J Magn Reson Imaging*. 2004;20:990-997.
110. Tsushima Y, Miyazaki M, Taketomi-takahashi A, Endo K. Feasibility of measuring human pancreatic perfusion In vivo using imaging techniques. *Pancreas*. 2011;40:747-752.
111. Taso M, Guidon A, Zhao L, Mortele KJ, Alsop DC. Pancreatic perfusion and arterial-transit-time quantification using pseudocontinuous arterial spin labeling at 3T. *Magn Reson Med*. 2019;81:542-550.
112. Cox EF, Smith JK, Chowdhury AH, Lobo DN, Francis ST, Simpson J. Temporal assessment of pancreatic blood flow and perfusion following secretin stimulation using noninvasive MRI. *J Magn Reson Imaging JMRI*. 2015;42:1233-1240.
113. Schawkat K, Ith M, Christe A, et al. Dynamic non-invasive ASL perfusion imaging of a normal pancreas with secretin augmented MR imaging. *Eur Radiol*. 2018;28:2389-2396.
114. Hirshberg B, Qiu M, Cali AMG, et al. Pancreatic perfusion of healthy individuals and type 1 diabetic patients as assessed by magnetic resonance perfusion imaging. *Diabetologia*. 2009;52:1561-1565.
115. Boushel R, Langberg H, Olesen J, et al. Regional blood flow during exercise in humans measured by near-infrared spectroscopy and indocyanine green. *J Appl Physiol*. 2000;89:1868-1878.
116. Raynaud JS, Duteil S, Vaughan JT, et al. Determination of skeletal muscle perfusion using arterial spin labeling NMRI: validation by comparison with venous occlusion plethysmography. *Magn Reson Med*. 2001;46:305-311.
117. Englund EK, Rodgers ZB, Langham MC, Mohler ER, Floyd TF, Wehrli FW. Simultaneous measurement of macro- and microvascular blood flow and oxygen saturation for quantification of muscle oxygen consumption: MRI measurement of muscle hemodynamics. *Magn Reson Med*. 2018;79:846-855.
118. Kumar K, Railton C, Tawfic Q. Tourniquet application during anesthesia: "what we need to know?". *J Anaesthesiol Clin Pharmacol*. 2016;32:424-430.
119. Englund EK, Langham MC, Ratcliffe SJ, et al. Multiparametric assessment of vascular function in peripheral artery disease: dynamic measurement of skeletal muscle perfusion, blood-oxygen-level dependent signal, and venous oxygen saturation. *Circ Cardiovasc Imaging*. 2015;8.
120. Wu W-C, Mohler E, Ratcliffe SJ, Wehrli FW, Detre JA, Floyd TF. Skeletal muscle microvascular flow in progressive peripheral artery disease. *J Am Coll Cardiol*. 2009;53:2372-2377.
121. Lopez D, Pollak AW, Meyer CH, et al. Arterial spin labeling perfusion cardiovascular magnetic resonance of the calf in peripheral arterial disease: cuff occlusion hyperemia vs exercise. *J Cardiovasc Magn Reson*. 2015;17:23.
122. Zheng J, Hasting MK, Zhang X, et al. A pilot study of regional perfusion and oxygenation in calf muscles of individuals with diabetes with a noninvasive measure. *J Vasc Surg*. 2014;59:419-426.
123. Grözinger G, Pohmann R, Schick F, et al. Perfusion measurements of the calf in patients with peripheral arterial occlusive disease before and after percutaneous transluminal angioplasty using Mr arterial spin labeling: perfusion measurement before and after PTA. *J Magn Reson Imaging*. 2014;40:980-987.
124. Englund EK, Langham MC, Li C, et al. Combined measurement of perfusion, venous oxygen saturation, and skeletal muscle T2* during reactive hyperemia in the leg. *J Cardiovasc Magn Reson*. 2013;15:70.
125. Baligand C, Hirschler L, Veeger TTJ, et al. A split-label design for simultaneous measurements of perfusion in distant slices by pulsed arterial spin labeling. *Magn Reson Med*. 2021;86:2441-2453.
126. Mathieu-Costello O, Hoppeler H, Weibel ER. Capillary tortuosity in skeletal muscles of mammals depends on muscle contraction. *J Appl Physiol*. 1989;66:1436-1442.
127. Kim ESH, Sharma AM, Scissons R, et al. Interpretation of peripheral arterial and venous Doppler waveforms: a consensus statement from the Society for Vascular Medicine and Society for vascular ultrasound. *J Vasc Ultrasound*. 2020;44:118-143.
128. Langham MC, Jain V, Magland JF, Wehrli FW. Time-resolved absolute velocity quantification with projections: projection-based velocity quantification. *Magn Reson Med*. 2010;64:1599-1606.
129. Englund EK, Rodgers ZB, Langham MC, Mohler ER, Floyd TF, Wehrli FW. Measurement of skeletal muscle perfusion dynamics with pseudo-continuous arterial spin labeling (pCASL): assessment of relative labeling efficiency at rest and during hyperemia, and comparison to pulsed arterial spin labeling (PASL): muscle perfusion with pCASL and PASL. *J Magn Reson Imaging*. 2016;44:929-939.

130. Wu W-C, Wang J, Detre JA, Ratcliffe SJ, Floyd TF. Transit delay and flow quantification in muscle with continuous arterial spin labeling perfusion-MRI. *J Magn Reson Imaging*. 2008;28:445-452.
131. Frank LR, Lu K, Wong EC. Perfusion tensor imaging: perfusion tensor imaging. *Magn Reson Med*. 2008;60:1284-1291.
132. Schraml C, Schwenzer NF, Martirosian P, Claussen CD, Schick F. Temporal course of perfusion in human masseter muscle during isometric contraction assessed by arterial spin labeling at 3T. *Magn Reson Mater Phys Biol Med*. 2011;24:201-209.
133. Wu W-C, Wang J, Detre JA, et al. Hyperemic flow heterogeneity within the calf, foot, and forearm measured with continuous arterial spin labeling MRI. *Am J Physiol-Heart Circ Physiol*. 2008;294:H2129-H2136.
134. Zheng J, Hastings MK, Muccigross D, et al. Non-contrast MRI perfusion angiosome in diabetic feet. *Eur Radiol*. 2015;25:99-105.
135. Boss A, Martirosian P, Claussen CD, Schick F. Quantitative ASL muscle perfusion imaging using a FAIR-TrueFISP technique at 3.0 T. *NMR Biomed*. 2006;19:125-132.
136. Marro KI, Hyyti OM, Kushmerick MJ. FAWSETS perfusion measurements in exercising skeletal muscle. *NMR Biomed*. 2005;18:322-330.
137. Marro KI, Hyyti OM, Vincent MA, Kushmerick MJ. Validation and advantages of FAWSETS perfusion measurements in skeletal muscle. *NMR Biomed*. 2005;18:226-234.
138. Duteil S, Bourrilhon C, Raynaud JS, et al. Metabolic and vascular support for the role of myoglobin in humans: a multiparametric NMR study. *Am J Physiol-Regul Integr Comp Physiol*. 2004;287:R1441-R1449.
139. Andreisek G, White LM, Sussman MS, et al. T2*-weighted and arterial spin labeling MRI of calf muscles in healthy volunteers and patients with chronic exertional compartment syndrome: preliminary experience. *AJR Am J Roentgenol*. 2009;193:W327-W333.
140. Schewzow K, Fiedler GB, Meyerspeer M, et al. Dynamic ASL and T2*-weighted MRI in exercising calf muscle at 7 T: a feasibility study. *Magn Reson Med*. 2015;73:1190-1195.
141. Elder CP, Cook RN, Chance MA, Copenhaver EA, Damon BM. Image-based calculation of perfusion and oxyhemoglobin saturation in skeletal muscle during submaximal isometric contractions: image-based oxyhemoglobin saturation in muscle. *Magn Reson Med*. 2010;64:852-861.
142. Zheng J, An H, Coggan AR, et al. Noncontrast skeletal muscle oximetry: skeletal muscle oximetry. *Magn Reson Med*. 2014;71:318-325.
143. Decorte N, Buehler T, de Almeida C, Araujo E, Vignaud A, Carlier PG. Noninvasive estimation of oxygen consumption in human calf muscle through combined NMR measurements of ASL perfusion and T_2 oxymetry. *J Vasc Res*. 2014;51:360-368.
144. Girard OM, Callot V, Robert B, Cozzone PJ, Duhamel G. MRI Perfusion MRI of the human cervical spinal cord using arterial spin labeling. *Proceedings of the 21st ISMRM Annual Meeting*. Salt Lake City, UT, USA; 2013:349.
145. Schraml C, Boss A, Martirosian P, Schwenzer NF, Claussen CD, Schick F. FAIR true-FISP perfusion imaging of the thyroid gland. *J Magn Reson Imaging*. 2007;26:66-71.
146. Solis-Barquero S, Aramendía-Vidaurreta V, Vidorreta M, et al. Multi-delay pseudo-continuous arterial spin labeling for perfusion quantification in the spleen. *Proceedings of the Joint Annual Meeting of ISMRM-ESMRMB*. London, UK; 2022:73.
147. Aramendía-Vidaurreta V, Solis-Barquero SM, Ezponda A, et al. Assessment of splenic switch-off with arterial spin labeling in adenosine perfusion cardiac MRI. *J Magn Reson Imaging*. 2022.
148. Li X, Metzger GJ. Feasibility of measuring prostate perfusion with arterial spin labeling. *NMR Biomed*. 2013;26:51-57.
149. Pretorius ES, Roberts DA. Continuous arterial spin-labeling perfusion magnetic resonance imaging of the human testis. *Acad Radiol*. 2004;11:106-110.
150. Artz NS, Wentland AL, Sadowski EA, et al. Comparing kidney perfusion using noncontrast arterial spin labeling MRI and microsphere methods in an interventional swine model. *Invest Radiol*. 2011;46:124-131.
151. Jacquier A, Kober F, Bun S, Giorgi R, Cozzone PJ, Bernard M. Quantification of myocardial blood flow and flow reserve in rats using arterial spin labeling MRI: comparison with a fluorescent microsphere technique. *NMR Biomed*. 2011;24:1047-1053.
152. Pohmann R, Speck O, Scheffler K. Signal-to-noise ratio and MR tissue parameters in human brain imaging at 3, 7, and 9.4 tesla using current receive coil arrays. *Magn Reson Med*. 2016;75:801-809.
153. Zuo Z, Wang R, Zhuo Y, Xue R, Lawrence KSS, Wang DJ. Turbo-FLASH based arterial spin labeled perfusion MRI at 7 T. *PloS One*. 2013;8:e66612.
154. Kashyap S, Ivanov D, Havlicek M, Huber L, Poser BA, Uludağ K. Sub-millimetre resolution laminar fMRI using arterial spin labelling in humans at 7 T. *Plos One*. 2021;16:e0250504.
155. Shao X, Guo F, Shou Q, et al. Laminar perfusion imaging with zoomed arterial spin labeling at 7 Tesla. *NeuroImage*. 2021;245:118724.
156. Snyder C, Delabarre L, Moeller S, et al. Comparison between eight-and sixteen-channel TEM transceive arrays for body imaging at 7 T. *Magn Reson Med*. 2012;67:954-964.
157. Li X, Auerbach EJ, van de Moortele PFV, Ugurbil K, Metzger GJ. Quantitative single breath-hold renal arterial spin labeling imaging at 7T. *Magn Reson Med*. 2018;79:815-825.
158. Li X, Johnson CP, Ellermann J. 7T bone perfusion imaging of the knee using arterial spin labeling MRI. *Magn Reson Med*. 2020;83:1577-1586.
159. Niess F, Schmid AI, Bogner W, et al. Interleaved 31P MRS/1H ASL for analysis of metabolic and functional heterogeneity along human lower leg muscles at 7T. *Magn Reson Med*. 2020;83:1909-1919.
160. Wang K, Shao X, Yan L, Ma SJ, Jin J, Wang DJ. Optimization of adiabatic pulses for pulsed arterial spin labeling at 7 tesla: comparison with pseudo-continuous arterial spin labeling. *Magn Reson Med*. 2021;85:3227-3240.
161. Ertürk MA, Raaijmakers AJ, Adriany G, Uğurbil K, Metzger GJ. A 16-channel combined loop-dipole transceiver array for 7T esla body MRI. *Magn Reson Med*. 2017;77:884-894.
162. Martirosian P, Boss A, Fenchel M, et al. Quantitative lung perfusion mapping at 0.2 T using FAIR true-FISP MRI. *Magn Reson Med*. 2006;55:1065-1074.
163. Boss A, Rempp H, Martirosian P, et al. Wide-bore 1.5 tesla MR imagers for guidance and monitoring of radiofrequency ablation of renal cell carcinoma: initial experience on feasibility. *Eur Radiol*. 2008;18:1449-1455.

164. Campbell-Washburn AE. 2019 American Thoracic Society BEAR cage winning proposal: lung imaging using high-performance low-field magnetic resonance imaging. *Am J Respir Crit Care Med*. 2020;201:1333-1336.
165. Taso M, Wollner U, Guidon A, et al. High spatio-temporal resolution 3D ASL renal perfusion with variable-density FSE and deep-learning reconstruction. *Proceedings of the 29th Annual Meeting of the ISMRM*. Vol 2349. Virtual; 2021.
166. Chen C, Qin C, Qiu H, et al. Deep learning for cardiac image segmentation: a review. *Front Cardiovasc Med*. 2020;7:25.
167. Bai W, Sinclair M, Tarroni G, et al. Automated cardiovascular magnetic resonance image analysis with fully convolutional networks. *J Cardiovasc Magn Reson*. 2018;20:65.
168. Hernandez-Garcia L, Aramendía-Vidaurreta V, Bolar DS, et al. Recent technical developments in ASL: a review of the state of the art. *Magn Reson Med*. 2022;88:2021-2042.

SUPPORTING INFORMATION

Additional supporting information may be found in the online version of the article at the publisher's website.

Table S1.: Lung ASL studies summary.
Table S2.: Placenta ASL studies summary.
Table S3.: Cardiac ASL studies summary.
Table S4.: Liver ASL studies summary.
Table S5.: Retinal ASL studies summary.
Table S6.: Pancreas ASL studies summary
Table S7.: Muscle ASL studies summary.

How to cite this article: Taso M, Aramendía-Vidaurreta V, Englund EK, et al. Update on state-of-the-art for arterial spin labeling (ASL) human perfusion imaging outside of the brain. *Magn Reson Med*. 2023;89:1754-1776. doi: 10.1002/mrm.29609